"Synthesis of MoS₂ and Nitrogen doped MoS₂ nanostructures as anode materials for Lithium Ion Batteries (LIBs)"

A Thesis submitted to

Indian Institute of Science Education and Research, Pune

In partial fulfilments of the requirements for the

BS-MS- Dual Degree Program,

Project by

Mr. Kanade Chaitanya Kaluram

Registration Number: 20131124

Department of Chemistry

Under the Guidance of

Supervisor,

Dr. Bharat B. Kale,

Director,

Centre for Materials for Electronics

Technology (C-MET), Pune.

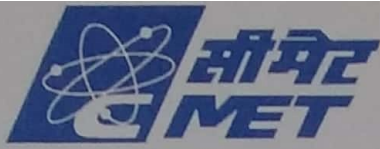**Co-Supervisor,**

Dr. Sudhir S. Arbuj,

Scientist,

Centre for Materials for Electronics

Technology (C-MET), Pune.

CERTIFICATE

This is to certify that this dissertation entitled "Synthesis of MoS_2 and Nitrogen doped MoS_2 nanostructures as anode materials for Lithium Ion Batteries (LIBs)", towards the partial fulfilment of the BS-MS dual degree programme at the Indian Institute of Science Education and Research, Pune represents study/work carried out by Kanade Chaitanya Kaluram at Centre for Materials for Electronics Technology, Pune. (C-MET, Pune) under the supervision of Dr. Bharat B. Kale, Director, C-MET, Pune during the academic year 2017-2018.

Kanade Chaitanya Kaluram

Roll no. 20131124

IISER, Pune.

Supervisor,

Dr. Bharat B. Kale

Director,

C-MET, Pune.

DIRECTOR
CENTRE FOR MATERIALS FOR ELECTRONICS TECHNOLOGY
(Dept. of Electronics & Information Technology, DeitY, Govt. of India)
Panchwati , Off Pashan Road, Pune - 411 008

Declaration

I hereby declare that the matter embodied in the report entitled "Synthesis of MoS_2 and Nitrogen doped MoS_2 nanostructures as anode materials for Lithium Ion Batteries (LIBs)" are the results of the work carried out by me at the Centre for Materials for Electronics Technology, Pune. (C-MET, Pune), under the supervision of Dr. Bharat B. Kale, Director, C-MET, Pune and the same has not been submitted elsewhere for any other degree.

Kanade Chaitanya Kaluram

Roll no. 20131124

IISER, Pune.

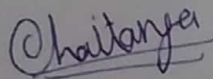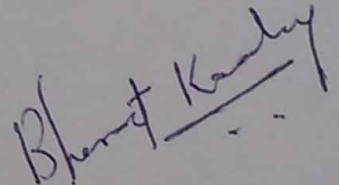Supervisor,

Dr. Bharat B. Kale

Director,

C-MET, Pune.

DIRECTOR
CENTRE FOR MATERIALS FOR ELECTRONICS TECHNOLOGY
(Dept. of Electronics & Information Technology, DeitY, Govt. of India)
Panchwati , Off Pashan Road, Pune - 411 008

ACKNOLWEDGEMENTS

Contents

List of Figures:

List of Tables:

Abstract

Lithium ion batteries (LIBs) have attracted lots of attention over last few years due to the high specific energy, high power density, longer life cycle and low self-discharge, making LIBs the advantageous over the conventional rechargeable lead acid batteries. Electronic systems are being reduced so that the system can accommodate more components for increasing reliability of electronic device and cheaper cost. The high power density batteries have important role in this miniaturization process. Use of nanomaterials can reduce the size of LIBs by increasing the power and energy density. Therefore, efforts has done to decrease the particle size of anode materials to nanoscale level.

Many efforts are in progress to find effective anodes for LIBs since the commercial anode for LIBs, graphite, has shown very limited capacity. In view of this, the project has been focused on development of indigenous raw materials as well as design and fabrication of lithium ion battery using the same nanomaterials. Among many different types of materials, molybdenum disulphide holds a great deal in LIBs technology as their structural resemblance with graphite structure and more theoretical capacity than graphite. The nitrogen-doped graphene has shown the promising result for increasing the capacity and power density of LIBs. Hence, attempts has been done to synthesise the nitrogen doped MoS_2, as nitrogen doped graphene has high processing cost.

The work has been presented in the form of four chapters. First chapter includes introduction of Lithium ion battery, literature survey, recent development in anode materials etc. Second chapter includes details of physicochemical and electrochemical characterization techniques, fabrication of LIBs, and detailed synthesis process for MoS_2 and nitrogen doped MoS_2 materials for lithium ion battery application. The third chapter includes the detailed discussion of results and characterization and the last chapter concludes the thesis.

The anode material has synthesized using the hydrothermal method to get the optimized morphology of the materials. The nitrogen doped MoS_2 nanostructures has been prepared for the first time in lithium ion battery applications. Different characterization techniques have been used to investigate the phase purity active materials. Morphological study performed shows flowerlike morphology of MoS_2 nanosheets and the size of the each petal is in the range of 20-80 nm depending on the amount of nitrogen doping in material. The MoS_2 electrode exhibits a high rate capability and structural stability even at very high Li-ion insertion−extraction current densities, which is comparable to other carbon materials.

CHAPTER 1: <u>INTRODUCTION</u>

1. LIBs

In modern world, rechargeable **Li-ion batteries (LIBs)** play a substantial role in energy storage applications because of its high power density, high gravimetric and volumetric energy, longer cycling life and low self-discharge property. [1-3]

In response to the need for better battery devices, the LIBs were perceived and developed. The LIBs replaced the conventional rechargeable batteries like lead acid and the primary manganese dioxide-zinc batteries. Due to its **high-energy density, good performance, and no memory effect**. LIBs have been largely used in portable electronics devices like mobile phone and portable laptops. [4-6] Recently, the application area has been more focused on battery-assisted hybrid electric vehicles. However, the manufacturing the high-energy storage device has been challenging work. It has required a combined approach and the improvement of performance by using new anodes, cathodes, and non-aqueous electrolytes to continue the steady development of high-energy lithium battery devices. To understand the functioning of LIBs first let us know the different components present in LIBs.

1.1 Components of Li ion battery

The three principal functional **components** of a **lithium-ion battery** are the positive electrode (Cathode on discharge) and negative electrode (Anode on discharge) and electrolyte. The positive and negative electrode were separated by separator membrane which allows to flow the Li ion from positive to negative electrode during charging and negative to positive electrode while discharging.

In this section, essential components of the LIBs have been discussed along with materials used for each components with their characteristic properties. For fabricating the LIBs, following components are required.
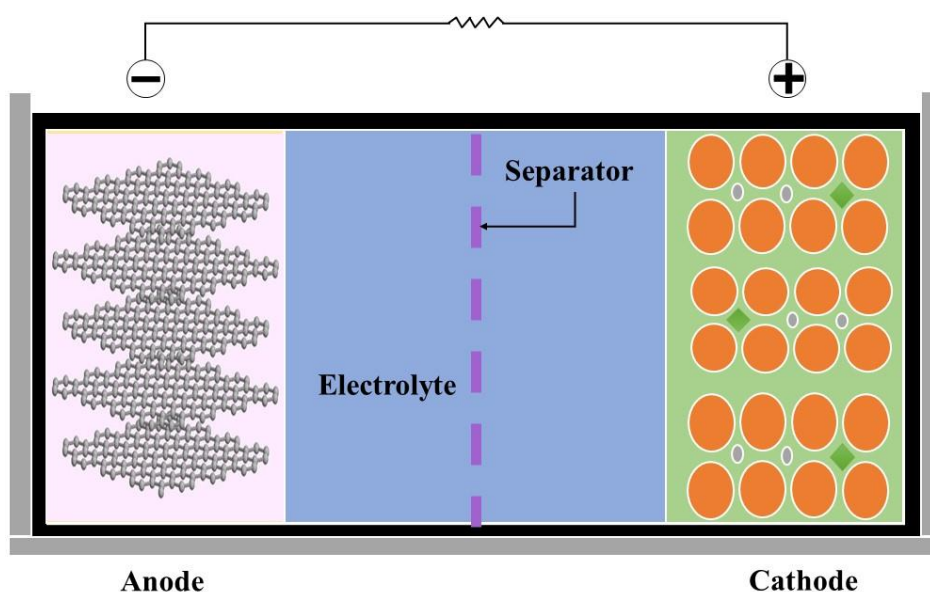
Figure 1.1 Schematic of Lithium Ion Battery

1.1.1 Cathode

The cathode is the positive electrode in the discharge cycle in rechargeable batteries. Cathode materials include lithium-metal oxides [such as $LiCoO_2$, $LiMn_2O_4$, and combination of lithium nickel manganese cobalt oxide $(Li(Ni_xMn_yCo_z)O_2)$], olivines (such as $LiFePO_4$), and layered intercalating oxides and sulphide materials. [7] $LiCoO_2$ is the most commonly used cathode material has been commercialised. Layered oxides of cobalt and nickel, intercalated with lithium ions are the most studied materials for lithium-ion batteries. They show a high stability in the high-voltage range, but cobalt has low abundance and it is toxic in nature, which is a tremendous disadvantage for battery engineering. Abundant and cheap manganese spinel can be used as cathode material even though they are substandard to layered compounds. Therefore, it is suitable as a cathode material in large-scale use of lithium-ion batteries. Manganese spinel shows a low-cost exchange along with a high thermal threshold and excellent rate capabilities but limited cycling behaviour. Therefore, mixtures of cobalt, nickel, and manganese are often used to combine the best properties and minimize the drawbacks. Olivines are non-hazardous and have a modest capacity with low fading due to cycling, but they lack conductivity.

Table 1.1 Practical capacity of different cathode materials [Ref.1]

Cathode material	Practical Capacity (mAh/g)
$LiCoO_2$	160
$LiNiO_2$	220
$LiNi_{0.8}Co_{0.2}O_2$	180
$LiNi_{0.8}Co_{0.15}Al_{0.05}O_2$	200
$LiMn_{0.5}Ni_{0.5}O_2$	160
$LiMn_{1/3}Ni_{1/3}Co_{1/3}O_2$	200
$LiMn_{0.4}Ni_{0.4}Co_{0.2}O_2$	200
$LiMn_2O_4$	110
$Li_{1.06}Mg_{0.06}Mn_{1.88}O_4$	100
$LiFePO_4$	160

Since the energy of a battery depends on the product of its voltage and its capacity, a battery with a higher energy density is obtained for a material with a higher voltage and a higher capacity. Thus, higher the cathode potential and larger the capacity of the cathode material, the higher the energy of the battery. Table 1 shows the comparison of practical capacity between different cathodic materials.

1.1.2 Electrolyte

The high working potential of LIBs can easily degrade the aqueous electrolyte present in cell. Hence it is important to select long lasting and safer electrolyte system for the fabrication of batteries. In general there are three types of electrolytes used in LIBs manufacturing. [7-9]

1.1.2.1 Liquid electrolytes

Liquid electrolytes in lithium-ion batteries contains the lithium salts, such as LiPF6, LiBF4, LiClO4 $LiBC_4O_8$ (LiBOB), $LiPF_6$, and $Li[PF_3(C_2F_5)_3]$ in an organic solvent, such as ethylene carbonate, dimethyl carbonate, and diethyl carbonate.[8] The choice of an electrolyte considers the compromise between flammability and electrochemical performance. Because the best performing solvents have rather lower boiling points and have a flash points around 30°C. Therefore, these batteries are at highest risk for danger and explosion. Decomposition of electrolyte and exothermic side reactions in LIBs to an effect known as **thermal runaway**. Thus, thermally stable ionic liquids can be considered as electrolyte materials but have major drawbacks, such as lithium dissolution out of the anode.

1.1.2.2 Polymer Electrolyte

Ionically conductive polymers are used as polymer electrolytes. The use of composites of polymers with ceramic nanoparticles results in higher conductivities and resistance to higher voltages. Polymer electrolytes can inhibit the lithium dendrites formation due to their quasi-solid and high viscous properties. [11]

1.1.2.3 Solid state electrolytes

Solid electrolytes fall into two main categories: ceramic and glassy. In ceramic solid electrolytes, ions conduct through ion transport channels, which are present due to ordered structure of ceramics. [12] Ceramic electrolytes includes the lithium super ion conductors (LISICON) and perovskites materials. In comparison with ceramics, glassy solid electrolytes are amorphous in nature and are of similar to ceramic elements, but have higher conductivity grain boundaries. [12]

In general, solid electrolytes shows a very poor low-temperature performance due mobility of lithium ion decreases at low temperature. In addition, solid electrolytes need specific conditions for deposition and temperature to achieve acceptable behaviour, which makes them extremely expensive, though they eliminate the requirement of separators and the risk of thermal runaway.

1.1.3 Separators

The separator physically separates the two electrodes from each other in order to avoid the short circuit. The separator soaks the liquid electrolyte and allows the ions to transfer through them from one electrode to other. A good separator must be an electronic insulator having minimal electrolyte resistance, strong mechanical strength, and chemical resistance to degradation in the highly electric potential. The advanced separator increases the safety by melting itself at higher temperature and restricts the ion flow through it i.e. **thermal shutdown**. Solid-state electrolytes and some polymer electrolytes does not require separator as they require direct contact with electrode to transfer the ions.

1.1.4 Anode

The anode is the electrode where oxidation is taking place in the battery, i.e. electrons get free and flow out of the battery during discharge. Carbon materials were mostly used as anodes due to their low cost and availability. Other than that lithium, lithium-alloying materials, and silicon are used as anode materials in LIBs. Lithium has charge density of 3862 mAh/g but shows problems with charge-discharge cycle and dendritic growth, which creates short circuits. Thus, it is not an ideal material for anode considering safety. Alloy anodes and intermetallic compounds shows the high capacities but volume change results in poor cycle repeatability.

Table 1.2 Theoretical capacity of different anode materials.

Anode	Theoretical Capacity (mAh/g)	Reference
Lithium	3862	7
Silicon	4200	13
Carbon nanotubes	1100	14
Carbon nanofibers	450	15
Graphene	960	16
Porous carbon	800-1000	17
SiO	1600	18
Germanium	1600	19
Tin	994	20
Transition metal oxides	500-100	21-23
Metal sulphides, phosphides, nitrides	More than 500	24-26

Silicon shows extremely high capacity of 4,199 mAh/g, matching with a composition of Si_5Li_{22}. However, it also goes through same poor cycling behavior and capacity fading problem. Along with these materials investigation has been done on germanium, SiO, tin, transition metal oxides, and metal sulphides to be consider as anodes in LIBs. However, to use them as effective anodes, limitations like capacity fading, volume expansion, poor electrical conductivity, and low coulombic efficiency has to be overcome first. In Table 2, different anodic materials are listed along with their theoretical capacity. Section 1.4 contains recent advancement and problems of different anode materials.

1.2 Principle and working of LIBs

In LIBs, lithium ions flow from anode to cathode during discharge cycle, converting chemical energy to electrical energy. Thus, LIBs consider as electrochemical cell. Let us look at the electrochemistry of LIBs

1.2.1 Electrochemistry

The electrochemical reactions takes place at the negative and positive electrodes in LIBs. During the reaction electrolyte act as a conductive medium for lithium ions to flow from one electrode to other. Electrical current establishes in external circuit when electron is withdrawn from anode and passed to cathode leading to discharging of lithium ion batteries.

The following reactions elucidates the chemistry at both electrodes during discharge. Here graphite and $LiCoO_2$ act as anode and cathode in lithium ion battery respectively.

Anode half reaction:

$$LiC_6 \longrightarrow 6C + Li^+ + e^- \qquad\qquad E° \sim 3\ V$$
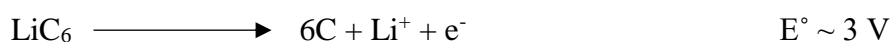
Cathode half reaction:

$$CoO2 + Li^+ + e^- \longrightarrow LiCoO_2 \qquad\qquad E° \sim 1\ V$$

Overall cell reaction:

$$LiC_6 + CoO_2 \longrightarrow LiCoO_2 + 6C \qquad\qquad E° \sim 4\ V$$
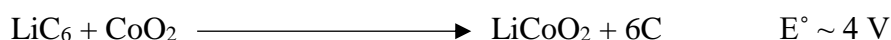
In the process lithium ion is intercalated into the electrodes leading to slight change in structure and volume of materials limiting the overall reaction.

During the first charging cycle the organic components present in liquid electrolyte decomposes at relatively high potential and forms the solid electrolyte interphase (SEI) on electrode. This interphase is electrically non-conducting but allows ionic mobility through it. Overall capacity of battery is reduces in this process but SEI layer formation can be diminished by coating the electrodes with carbon materials.

1.2.2   Charge-Discharge cycle

During discharge, the lithium ions (Li^+) move from the negative electrode to the positive electrode through the electrolyte and separator membrane while the electrons flow through the external circuit in the same direction. For charging, an external voltage applied to lithium ion battery which withdraws the electron from positive end and pass it to the negative electrode of battery through external circuit.(Polarity of electrodes in battery is not changed during the charging.) During charging Li^+ flows from positive electrode to negative electrode to complete the circuit. It is mandatory to apply the higher voltage than battery voltage to charge the battery during charging process.

Discharging of battery can be considered as spontaneous process while charging, battery goes under three important phases. In constant current phase, constant current is applied to battery until each cell voltage steadily reaches to its maximum voltage. Balanced phase of battery is achieved by reducing the current and levelling the state of charge (SoC) of the each cell through balancing circuit. In the last phase, constant voltage equal to maximum voltage of battery is applied until circuit current is reached to its set value.
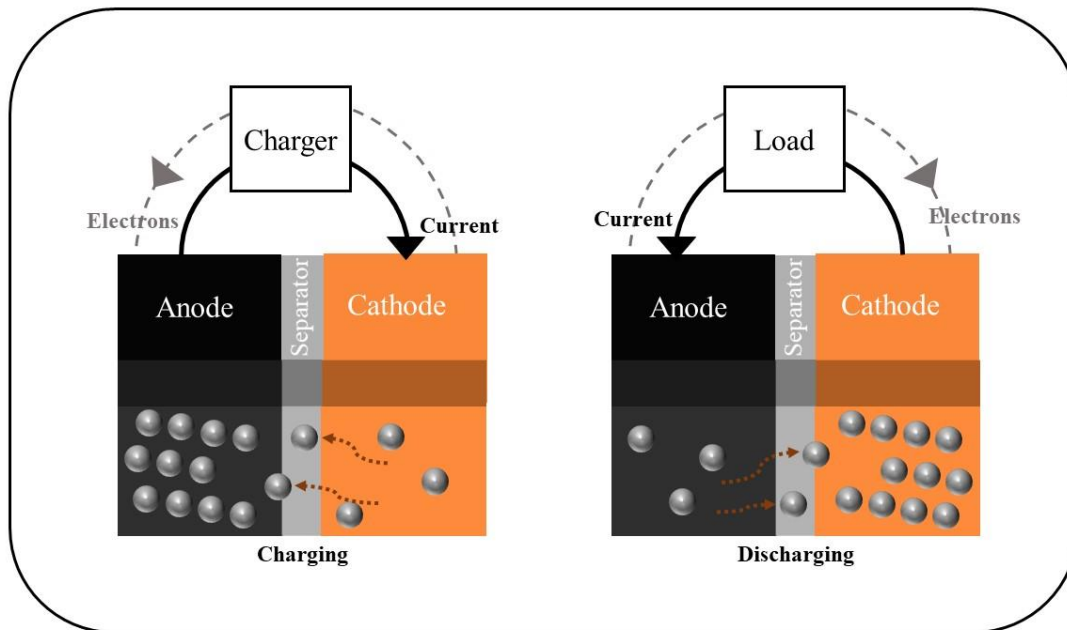
Figure 1.2 Charge-Discharge cycles of lithium ion battery.

1.2.3 Performance

Performance of battery depends on its specific energy density, cycling repeatability, cycle life, cell voltage, power density etc. The voltage and energy density of battery is mostly influenced by properties of electrode materials. As there are many materials available for the positive and negative electrode of LIBs, there is variation in working voltage and energy density in LIBs.

Compared to conventional lead-acid, Ni-MH, and Ni-Cd batteries, LIBs shows good performance, higher energy density and open circuit voltage. LIBs are prone to some issues like capacity fading, poor cycling performance, high risk of explosion and internal resistance. These problems leads to voltage drop across the electrodes subsequently lower current and capacity. LIBs are known for their thermal runway problem but these problems can be minimised by thermal shutdown mechanism.

The different combination of anode and cathodes of lithium ion battery can give voltage upto 5 V. The recharging time of LIBs has reduced from 2 hours to 15 minutes for 3000mAh battery over the few years of research and development of LIBs. Thus, Lithium ion batteries have huge potential in industrial application as well as developmental research of battery.

Different parameters of measurements are the result of different material properties. Cell potential, capacity, power and energy density are related to the intrinsic property of the electrode materials. The cycling life and lifetime depend on the nature of the interfaces between the electrodes and electrolyte. Moreover, safety is related to the stability of the electrode materials and interfaces. Here are some basic parameter to check the battery performance.

1.2.3.1 Voltage

The driving force of a chemical reaction is the decrease of Gibbs free energy of the system, which is expressed as:

$$\Delta G° = -nFE°$$

Here n is the number of electrons involved in the stoichiometric reaction; F is Faraday Constant, the charge on one mole of electrons (96,500 C); $E°$ is the standard potential, voltage between the two electrodes. The reduction potential may change according to concentration and temperature when they are different from the standard conditions, as expressed by the Nernst equation:

$$E = E° + \frac{RT}{F} \, ln\frac{[a \, oxi]}{[a \, red]}$$

The voltage of a battery can be calculated from standard potentials as follows:

Voltage of a battery= Cathode (reduction potential) – Anode (reduction potential)

1.2.3.2 Specific Capacity

The theoretical capacity of a battery is defined as the total quantity of electricity involved in the electrochemical reaction and is defined in terms of coulombs (C) or ampere-hours (Ah). The specific capacity is a characteristic of the material defined as the amount of charge transfer during reaction normalized by the mass or by the volume of the active material, known as gravimetric or volumetric specific capacity, respectively. People use different terms depending on whether weight or size is more important in the battery application. Specific capacity may change during cycling. Cycling stability is an important parameter in the battery performance evaluation.

The reversibility of the lithiation process is characterized by Coulombic efficiency

$$CE\% = \frac{Cdc}{Cc} \times 100$$

Here C_c is the charge specific capacity and C_{dc} is the discharge specific capacity at the same cycle.

1.2.3.3 Energy

The energy that a battery can deliver is defined in terms of Watt Hour (Wh) and can be calculated as follows:

$$E = V.C$$

Here C is the discharge capacity; V is the average potential of electrochemical reaction during discharge. The specific energy or energy density is used more often and gravimetric specific

energy is in the unit of Watt Hour per Kilogram (Wh/kg) while volumetric specific energy is in the unit of Watt Hour per Litre (Wh/L).

1.2.3.4 Power

Power is use to identify how fast the battery can charge or discharge. It is defined as:

$$Power = Voltage \ x \ Current \ rate$$

Here Current rate is the current per unit mass of the active material per second. Batteries that can function under higher power will better meet today's demand of technology.

1.3   Effect of nanosize on electrode materials.

Lithium ion battery suffers from problems like capacity fading, poor electrical conductivity, volume expansion and low columbic efficiency. Thus, battery electrodes have to overcome this limitation to be a perfect anode or cathode material for battery. These problems are mainly related with low electrode/electrolyte interface and surface area availability to for Li^+ to interact with electrode materials. Thus, use of nanostructures of listed materials can improve the performance of battery by solving these crucial problems. These nanosized materials can help to achieve the theoretical values to develop the technological effective batteries. [27-30]

The main advantages of using nanotecgnology in LIBs are given below. [30-34]

i)   The nanomaterials provides high surface to volume ratio. Thus, capacity of the material enhances due to availability of large number of active sites for lithium storage.

ii)   The high surface area in nanomaterials increase effective contact area with electrolyte leading to enhancement in electrode/electrolyte interface.

iii) Diffusion pathway for lithium ion reduces which enhances the power capability of battery.

iv)   Electrochemical reactions which are limited in bulk material can be triggered at nanoscale level of that material.

1.4   Recent advancement in anode materials.

This section contains the recent development and nanotechnology research on anode materials for batteries depending on their performance and applications.

1.4.1   Carbon materials

Carbon materials are the excellent choice for the anode material as they features the property like thermal and electrochemical reaction stability, lithium ion intercalation and low cost processing. [35-37] Along with that, carbon coating on other electrode materials decreases the SEI formation leading to enhancement in capacitive properties of lithium ion battery. Carbon materials reduces the electrolyte decomposition and formation of HF. In batteries HF produces

when $LiPF_6$ reacts with moisture and it can decompose the transition metals in batteries leading to capacity decay. Carbon materials reduces this process and increases the life of the battery. Carbon anode materials are available in two categories i.e. SOFT carbon and HARD carbon. SOFT carbon have properly stacked structure while HARD carbon is in disoriented state. SOFT carbon can show the reversible capacity between 350 to 370 mAh/g and HARD carbon show the reversible capacity between 200 to 600 mAh/g. [37-42] Nevertheless, both of the carbon have some limitations, SOFT carbon shows the high voltage hysteresis and low capacity during delithiation and HARD carbon have low initial coulombic efficiency. [43]

At the nanoscale level, carbon nanotubes have theoretical reversible capacity of 1116 mAh/g. The best performing carbon nanotubes have shown the capacity of 1050 mAh/g whit low coulumbic efficiency. [44-46] However, mass production and cost of production is still challenge to industry. Among the all, graphene seems to be most feasible solution for anode materials as few layers of graphene can give the theoretical capacity of 1116 mAh/g.[47,48] There is reach amount of literature is available about graphene as LIBs anode material. Present research activity is focused on hybrid graphene/metal or semiconductors or graphene/metal oxides and sulphides. The SnO_2 particle/nitrogen doped graphene has shown the gravimetric capacity of 1220 mAh/g over 100 cycles. [49]

1.4.2 Metal sulphides

The transition metal sulphides are important anode materials for LIBs as they have higher capacity than graphite. Metal sulphides also suffers from poor cycling stability, large volume change and low rate performances. They are prone to electrode pulverisation leading to slow charge transfer and unstable SEI layer formation. These difficulties with metal sulphides can be easily diminished by using their nanostructure forms. Thus, metal sulphides can be considered as promising anode materials for battery applications. The composite formation of metal sulphides with carbon has shown the enhancement in cycling stability and rate performance.

The various transition metal sulphides are explored as anode materials for LIBs. Rock salt type MnS can show the discharge capacity upto 1300mAh/g however after 20 cycles the capacity decreases to 400-600 mAh/g.[50] FeS and FeS_2 can show the higher capacity than 500 and 600 mAh/g respectively.[51,52] The layered metal sulphides have advantage over others as they show the low volume expansion compared all other anode materials after the lithiation. The capacity and performance of layered metal sulphides electrode is greatly influenced by the morphology and particle size of the nanostructures. MoS_2 is one of the best candidate among the layered structure for battery application. Hydrothermally synthesised MoS2 have shown

the 74% capacity retention after 70 cycles from 791 to 585 mAh/g at 100 mA/g current density.[53] The hierarchical MoS2 nanospheres assembled units showed the highest specific capacity of 1183.5 mAh/g and retention of 905.3 mAh/g after 50 cycles.[54] Thus, in this project we chose to work on MoS_2 nanoparticles as they have shown so much potential for LIBs. In next section will introduce the different properties and structure of MoS_2.

1.5 Molybdenum disulphide (MoS2)

Molybdenum disulphide (MoS_2) is an inorganic compound comes under transition metal dichalcogenide family compounds. It is silvery black in appearance and relatively unreactive. MoS_2 has similar appearance and layered structure like graphite. Bulk MoS_2 is indirect bandgap semiconductor with a bandgap of 1.23 eV and diamagnetic in nature. [55]

MoS_2 is a layered structure in which a plane of molybdenum atoms is packed in the planes of sulphide ions. These monolayers of MoS_2 are held together by week van der Waals forces to form the many-layered structure similar to graphite. MoS_2 is found in three crystallographic phases, 2H-MoS_2, 3R-MoS_2, and 1T-MoS_2, where the "H", "R" and "T" indicate hexagonal, rhombohedral and tetragonal symmetry, respectively. 2H and 3R phase of MoS_2 are semiconducting while 1T is metallic in nature. 1T is metastable phase and can be easily converted in stable 2H or 3R phase. *(Picture Credits: DOI: 10.1038/NNANO.2012.193)*
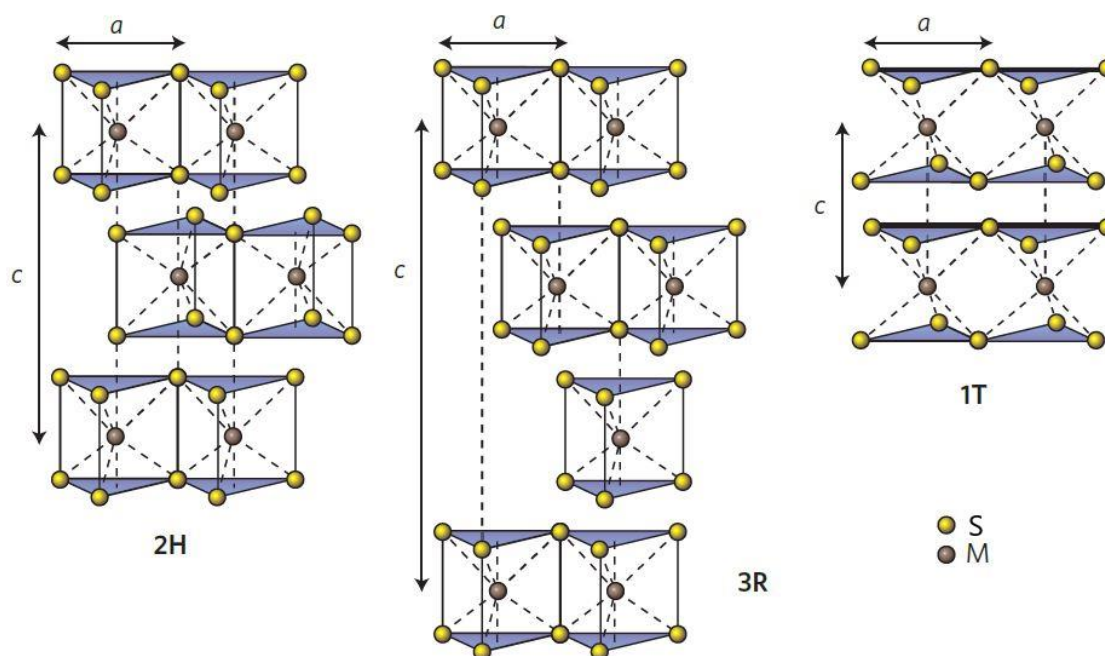
Figure 1.3 Crystal structures of 2H, 3R, and 1T molybdenum disulphide

The different properties of MoS_2 can have different application in industries. MoS_2 have low friction coefficient due to weak van der Waals interactions between the two layers. Thus, MoS_2 uses as dry lubricant in high temperature machines. MoS_2 is efficient catalysts for hydrogen evolution by water splitting. MoS_2 has been considered as a component of photo electrochemical applications and for microelectronics applications. MoS_2 has been used as a flexible transistor and component of circuits. MoS_2 also possesses mechanical strength, electrical conductivity, and can emit light, which can be used as photodetectors. MoS_2 also shows the higher theoretical capacity than graphite. The main difficulty in using the MoS_2 electrode in energy storage application is its low rate performance and capacity fading. [56] Use of nanomaterials and doped materials can enhance the electrochemical performance of MoS_2 to overcome these capacitance problems. There are reports demonstrating the enhancement in electronic properties of MoS_2 by doping the transition metals in it. [57, 58] Nevertheless, non-metal doping of MoS_2 increases the performance of lithium ion batteries has not yet been reported. The nitrogen-doped graphene has shown the enhanced performance for lithium ion battery and other energy storage devices. [59-61] Therefore, nitrogen doped MoS_2 could be expected to show the enhanced performance for electrode of lithium ion battery as MoS_2 sheets shows the much resemblance with graphene.

1.6   Objective of the thesis

The main objective of thesis are as follows:

I.   Synthesis of MoS_2 and nitrogen doped MoS_2 nanostructures using hydrothermal reaction techniques.

II.   To characterise the prepared MoS_2 and nitrogen doped MoS_2 nannostructures using various techniques such as, X-ray diffraction, UV-Visible absorbance, electron microscopy like FESEM and TEM, and Raman spectroscopy technique.

III.   Fabrication of the lithium ion battery using prepared MoS_2 as anode material.

IV.   Detailed Electrochemical Characterization of lithium ion cells such as CV, Impedance, Efficiency, capacity study, cyclability testing of electrode materials for Li^+ storage ability.

V.   The electrode stability study including coulombic efficiency, cycling stability, and rate capability of all the electrodes and its characterization.

1.7   Outline of thesis

Chapter 1: Introduction

This chapter deals with the brief introduction about the lithium ion batteries (LIBs) and its basic working principle. Further in this chapter the advantages of LIBs over other conventional energy storage devices and important challenges in LIBs is discussed. Furthermore, recent development and research on anode materials and their practical problems are discussed. The general information about the molybdenum sulphide anode material is given in this chapter. At the end of the chapter objective and outline of the thesis is given.

Chapter 2: Experimental, Characterisation techniques, and Fabrication of LIBs.

This chapter describes the synthesis route like hydrothermal and sol-gel method, along with their fundamentals. A detailed experimental procedure involving hydrothermal route method is described which is used in present work. This chapter also describes the principle and working of different characterisation techniques like XRD, UV-Visible spectroscopy, FESEM, TEM, and Raman spectroscopy. All these techniques were used for physical and chemical analysis of prepared MoS_2 nanomaterials. Further, the fabrication process of LIBs and battery parameter measurement have been discussed.

Chapter 3: Result and Discussion

This chapter includes the detailed discussion on characterisation results of hydrothermally prepared MoS_2 nanomaterials and nitrogen doped MoS_2 nanostructures. The optimisation of MoS_2 nanostructures is discussed based on yield, XRD, and FESEM. The successful doping of nitrogen is confirmed by various characterisation techniques such as XRD, FESEM, TEM etc. The effect of nitrogen doping on the physical, chemical and optical properties of the MoS_2 is discussed in this chapter. Finally the detailed discussion about fabricated lithium ion battery is given with results.

Chapter 4: Conclusion and Future Scope

This chapter briefly concludes the performed research work followed by future scope of the MoS_2 nanomaterials.

CHAPTER 2: <u>METHODS</u>

This chapter includes, brief introduction to different synthesis techniques, which are used for synthesising nanomaterials. These methods include hydrothermal, solvothermal, and sol-gel etc. along with their fundamentals. The hydrothermal method, which is used for synthesis of MoS_2 nanomaterial in the present work is described in detailed. This chapter also describes principles and working of all the characterization techniques, which are used to study the synthesized nanomaterial such as X-ray diffraction (XRD), UV-visible absorbance, field emission scanning electron microscopy (FESEM), transmission electron microscopy (TEM), and Raman spectroscopy. All this techniques were utilized to investigate the optical, physical and chemical properties of the synthesized nanomaterials. Further, the lithium ion battery fabrication process along with the battery parameter measurements has been discussed.

2.1 Techniques for the synthesis of nanomaterials.

There are many techniques has been reported to synthesis the nanomaterials for different kind of application. [62] Nanomaterials shows different physical and chemical properties depending on their size and synthesis method. [63, 64] There are two different ways to synthesize the nanomaterials i.e. top-down and bottom-up approach. Figure. 2.1 explains both the approaches [65]. In top- down approach, the bulk materials are divided physically or chemically until they get a preferred size of interest [66]. In this approach, surface structural defects, internal stress and contamination can occurs due to the extreme conditions, which are used for synthesis of nanoparticles. This effect on physical properties and morphologies of the nanomaterials. [67] Top down approach includes the various types of physical and chemical techniques such as ball milling, exfoliation, cutting, etching, grinding etc.

The bottom-up approach includes the synthesis of nano or micron sized materials by accumulating atoms or molecules or supramolecular templates. Bottom up approach has been well accepted and more applicative in the fabrication and processing of nanostructure materials than the top-down approach [67].

Following are the different synthesis methods for semiconductor nanomaterials applied in the present thesis.
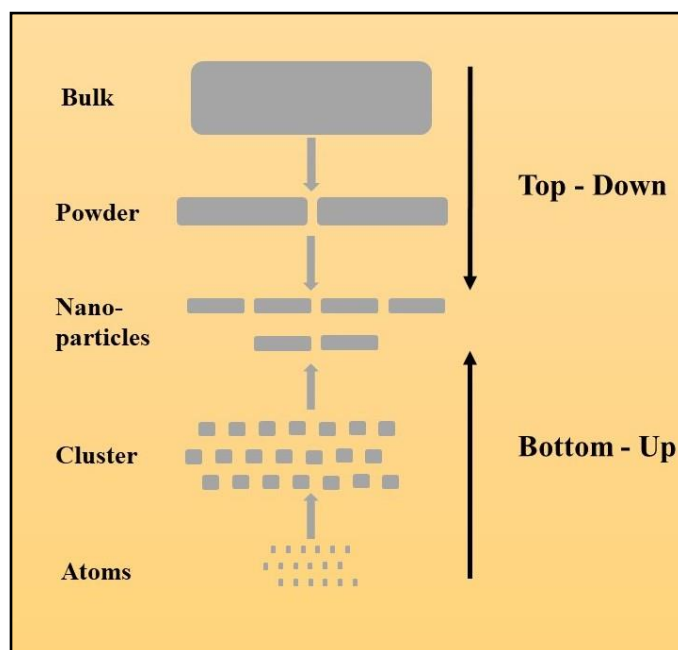
Figure 2.1 Schematic of Top-Down and Bottom-Up approach.

2.1.1 Sol-gel method

Sol Gel process is wet-chemical technique also known as chemical solution deposition. Nanomateriales typically metal oxides synthesized by this technique in which sol is a precursor for the formation of an integrated network of discrete particles or polymer known as a gel. [68, 69] Metal alkoxides or chlorides in the solution state undergo hydrolysis and polycondensation reaction to form network of either elastic solid or colloidal dispersion. A system composed of discrete sub micrometer particles dispersed to various degrees in a host fluid. Metal-oxy or metal-hydroxy polymer is formed in solution due to sol transformed into gel like heterogeneous mixture containing liquid as well as solid phase by hydrolysis or a polycondensation reaction whose morphologies ranges from discrete particles to continuous polymer network. Hydrolysis lead to formation of sol and dispersion of colloidal particles in a liquid and further condensation results into gel which is an interconnected, rigid and porous inorganic network enclosing a continuous liquid phase. This transformation is called sol-gel transition. Gel drying can be performed in two ways, i) Removal of liquid trapped in pores under hypercritical conditions in which network does not collapse and aerogels are produced. ii) The gel is dried under ambient condition due to this densification and shrinkage of pores occur yielding xerogel. Porosity generated in the gel depends upon the rate of solvent evaporation. The dried gel is fired or thermally treated at desired temperature to form metal oxides. The precursor sol can be deposited on a substrate to form a film by dip coating or spin coating. Precursor sol can also be casted into a suitable container with the desired shape to

obtain monolithic ceramics, glasses, fibres, membranes and aerogels. The nanopowders can be synthesized from precursor gel.
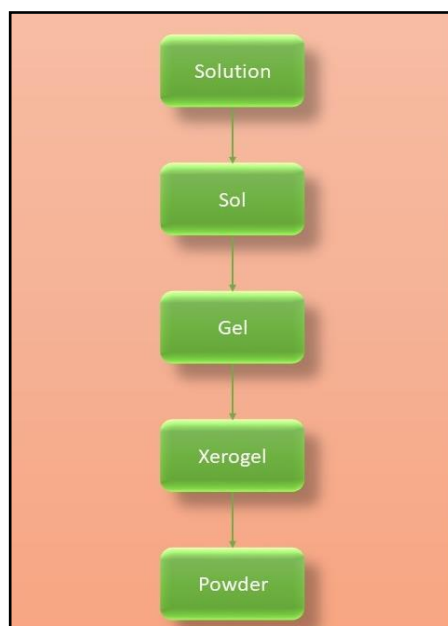
Figure 2.2 Sol-gel method for synthesis of nanomaterials.

Sol gel synthesis is a low temperature and cheap method that allows control over the chemical composition. Small amounts of the dopant can be added into the sol and end up uniformly dispersed in the product. The material synthesized by sol gel technique has various applications in electronics, energy, space, sensors and medicines. The major drawback of sol gel method is control over the rate of hydrolysis and condensation of molecular precursors. These reactions are too fast, resulting in loss of morphological and structural control over the oxide materials. Besides, the different reactivity of metal oxides makes it difficult to control the composition and uniformity of the complex multiple oxides by a sol gel process. The control over the reactivity of the precursors can be attempted by i) use of organic additives and capping agents like carboxylic acids, β-diketones or functional alcohols, which acts as chelating ligands and modify the reactivity of the precursors and ii) control over the solvent concentration and the hydrolysis of metal oxide precursors. In spite of all these efforts, the stronger sensitivity of aqueous sol gel process towards any slight changes in the synthesis conditions and the simultaneous occurrence of hydrolysis and condensation reaction make it still impossible to complete control over the sol-gel processing of metal oxides in aqueous medium.

In non-aqueous sol-gel synthesis, the transformation of reactants takes place in an organic solvent under exclusion of water. The potential precursors include inorganic metal salts, metal

alkoxides, metal acetates and metal acetyl acetonates etc. Organometallic compounds are also frequently used, but the process is rather based on thermal decomposition than sol-gel.

2.1.2 Hydrothermal / Solvothermal synthesis method

The reactions occurring under the conditions of high-temperature and high-pressure (>100ºC, > 1 atm.) in aqueous solutions in a closed system are known as hydrothermal reactions. [69] The hydrothermal method is advantageous due to ability of creating different crystal phases, which are unstable at the melting point as compared to other conventional synthesis methods. The nanomaterials with high vapour pressure close to the melting point can also definitely produce with this technique. The use of other organic solvents instead of water changes this method in to solvothermal. In this process, the starting materials are insoluble at room temperature, but high temperature and pressure give rise to solubility and energy for completion reaction. Therefore, in solvothermal method solvent is not limited to, water

Figure 2.3 Autoclave for hydrothermal synthesis of nanomaterials.

but it also includes many polar and nonpolar organic solvents. In case of hydrothermal method, the solvent water may produce oxides by reacting with the precursors, which cannot happen in case of solvothermal technique. [70] Use of a combination of different organic solvents and water, suppress the melting point of many materials for easy and fast processing.

Due to a solvent evaporation phenomenon, variety of surface morphology can be seen in recent research articles by using a hydrothermal process. The photograph of hydrothermal reactor also called as autoclave is shown in Figure. 2.3, It contains stainless steel (SS) container and teflon cup which can be fitted inside the SS container having capacity to withstand high temperatures and pressures for longer time. The use of this technique for synthesis of one dimensional (1D), 2D, and hierarchical nanostructures have been reported.

The morphology depends on the choice of solvent, capping agent or surfactants, reaction temperature, additives and pH of the reaction mixture. [71] Overall this technique provides control growth rate for nanostructures. On the other side only disadvantage of this technique is the cost and safety of the hydrothermal reactor.

2.2 Experimental

2.2.1 Synthesis of molybdenum disulphide (MoS₂) nanomaterial.

For the synthesis of hexagonal (2H) phase MoS_2 nanostructures, the ammonium heptamolybdate tetrahydrate (Sigma-Aldrich), thiourea (fisher scientific), and deionised water were used without further purification.

In typical experimental procedure, ammonium heptamolybdate tetrahydrate and thiourea were used as molybdenum and sulphur precursor to synthesis the MoS_2 respectively. A mixture of ammonium heptamolybdate tetrahydrate and thiourea in 60 or 30 ml of water were prepared by keeping the moles ratio of Mo:S as 1:M (M = 2.5, 4, 8). Then this mixture transferred to teflon lined stainless steel autoclave. The sealed autoclave were kept at 200˚C for TT (TT = 03, 06, 12, 24, 48, 72) hrs in hot air oven. The obtained reaction product was washed with water and ethanol to get black coloured MoS_2 powder. MoS_2 nanostructure were optimised according to required morphology and phase.

2.2.2 Synthesis of nitrogen doped MoS₂ nanomaterials.

The optimised MoS_2 powder in Section 2.2.1 were heated in tube furnace under nitrogen environment at 400˚C for 4 hrs to get nitrogen doped MoS_2. The obtained product were termed as MoS_2 400. Further, to increase the amount of doping MoS_2 400 were mixed with urea (fisher scientific) in the weight ratios of 1:1, 1:3 and 1:5 subsequently heated in tube furnace at 400˚C for 30 min under nitrogen environment and obtained products were termed as MoS_2 N1, MoS_2 N3, and MoS_2 N5 respectively.

The prepared MoS_2, MoS_2 400, MoS_2 N1, MoS_2 N3, and MoS_2 N5 nanostructures were characterised by different techniques and used for fabrication of lithium ion coin cell.

2.3 Characterization Techniques

In addition to conventionally available characterization techniques, the characterisation of nanostructured materials is largely facilitated by the advances in surface analysis techniques. In this section, the different characterisation techniques that have been employed to characterize the synthesised nanomaterials and their nanocomposites under investigation in this thesis have been described in brief. The scope of the discussion is focused specifically on

the basic and the fundamental principles of the characterization techniques used. General standard operating procedures, instrumentation and technical details have not been covered here, as enormous literature is already available on the same.

2.3.1   X-Ray diffraction (XRD)

XRD is widely used for characterization of nanomaterials. It is a nondestructive technique used for detection of crystallinity, crystal structures, and the lattice constant of materials. Each crystalline material gives a specific XRD pattern i.e. the same material always gives the same pattern; and in a mixture, each produces its pattern irrespective of the others. The X-ray diffraction pattern of a pure substance can be consider as "characteristic" of the substance. The powder diffraction technique is ideal for identification and characterization of polycrystalline phases in material. An electron in an alternating electromagnetic field will oscillate with the same frequency as the field. When an X-ray beam falls on an atom, the electrons in the atom start to oscillate with the identical frequency of the incident X-ray beam. We will have destructive interference in every direction, because waves are out of phase and there is no resultant energy leaving from the solid sample. However, the atoms in a crystal are periodically arranged, because of that it is possible to have constructive interference along few directions. The waves will be in-phase and there will be well-defined X-ray beams leaving the sample at particular directions. Therefore, a diffracted beam is composed of a large number of scattered rays conjointly supporting one another. In X-ray diffractometer, a collimated beam of X-rays with a typical wavelength is incident on the sample and is diffracted by the crystallite phases in the specimen according to Bragg's law: [64]

$$n\lambda = 2d \sin\theta$$

Where 'n ' is the order of diffraction, 'd' is distance between planes in the crystalline phase and 'λ' is the wavelength X-ray generated. The amount of X-rays diffracted is measured as a function of the diffraction angle 2θ and orientation. The diffraction pattern is used to identify the material's crystalline phases and to measure the crystallite structure.

2.3.2   UV- visible spectroscopy

Optical absorption spectroscopy (UV-Vis. Spectroscopy) is a method to study metals, semiconductors and insulators in bulk, thin film, nanostructures etc. Semiconductors and insulators shows an optical energy gap. The absorption of the wavelength takes place, when there is sufficient amount of energy to excite the electron from valence band to conduction band. At shorter wavelengths or higher energy, photons continue to absorb. The absorbed (or

reflected) intensity as a function of wavelength from ultraviolet (200 nm) to infrared (3000 nm
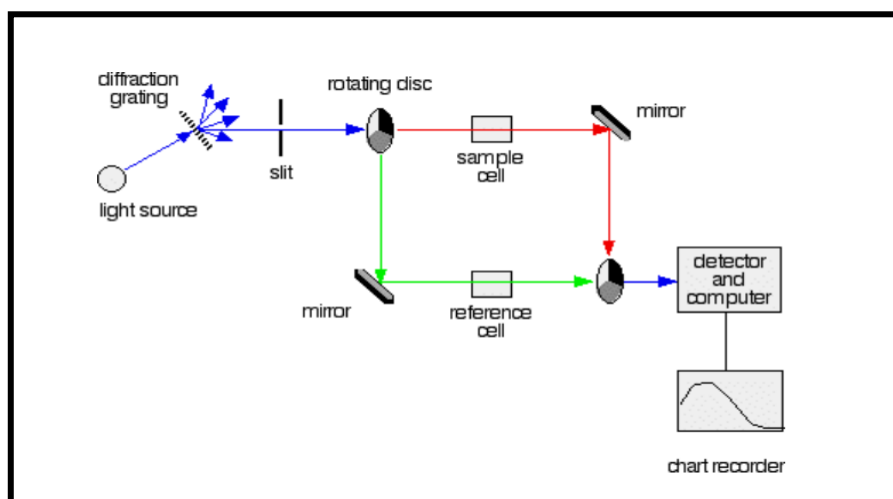
Figure 2.4 Instrumentation of UC-Visible spectrometer. (Picture Credits: https://www.chemguide.co.uk/analysis/uvvisible/spectrometer.html)

or many times up to 1000 nm) is useful to know electronic structure and transitions between valence and conduction band of materials. With reduction in the particle size, the absorption edge shifts toward lower wavelengths and it is known as blue shift. [64]

2.3.3 Field Emission Scanning Electron Microscopy (FESEM)

FESEM is used to study the small surface and morphological details of the materials and objects. In case of FESEM equipment electrons emits from a field emission source and accelerate in a high electrical field. Electronic lenses focuses the primary electrons in to a narrow scan beam that bombards the object. The secondary electrons are emits from object surface due to bombardment. [64] The angle and velocity of these secondary electrons plays the crucial role to get the surface structure and morphology of the object.

Electronic signal is produced by the detector by detecting the secondary electron emitted from the material. This signal is amplified and converted to image on a monitor processed further.

2.3.4 Transmission Electron Microscopy (TEM)

In TEM, electrons accelerated at 100 KeV or higher upto 1 MeV are projected onto the thin specimen of the sample, penetrating the sample either deflected or straight. The type of information obtained from a particular sample depends solely on the scattering processes of the electron when they passing through the material. Elastic scattering gives rise to diffraction patterns. The magnification or resolution of all TEM is a depends on the small effective electron wavelengths "λ" which is given by de Broglie's relationship: [64]

$$\lambda = \frac{h}{\sqrt{2mqV}}$$

Where, m is electron mass, q is charge, h is Planck's constant, V is potential difference through which electrons are accelerated. In accordance with this equation, it can be inferred that higher the operating voltage, the greater its lateral spatial resolution. [64] By using high voltage TEM instruments, it is possible to image thicker samples due to greater penetration depth and less interaction of the high voltage electrons with the specimen. Limited depth resolution is the inherent problem with TEM.
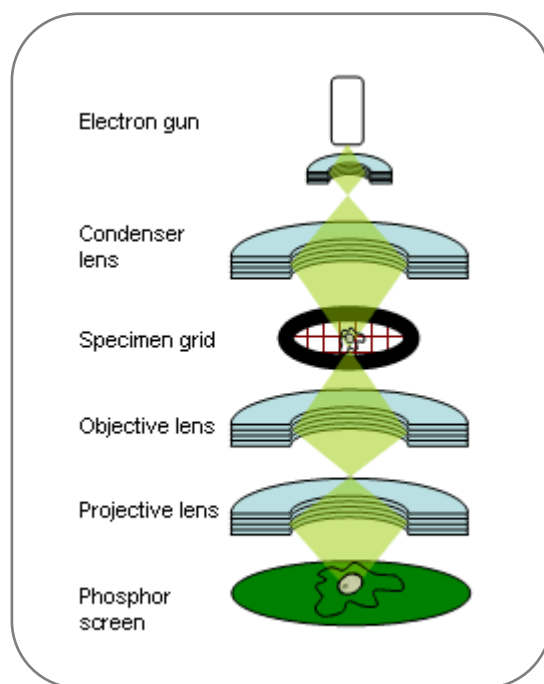
Figure 2.5 Schematic of Transmission Electron Microscopy (TEM).

(Picture Credits: http://frimat.unifr.ch/frimat/fr/page/485/)

Selected-area diffraction (SAED) in TEM offers competence to identify and determine the crystal structure of individual nanomaterials and super lattices. It also helps to identity polymorphs if present in the material. In SAED, a selected area aperture is used to limit the diffracting volume. SAED patterns can be used for detection of the Bravais lattices and lattice parameters of crystalline materials, similar to XRD pattern analysis.

In addition to its structural and chemical analysis capabilities, TEM has been used for a few spin-off applications in nanotechnology. Examples include determination of melting points of nanomaterials in correlation to disappearance of electron diffraction and measurement of mechanical as well as electrical properties of nanowires and nanotubes.

2.3.5 Raman Spectroscopy:

Raman scattering is the inelastic scattering of a photon by molecules, which are excited to higher vibrational or rotational energy levels. A transparent substance scatters the some portion of light when light is incident on it. In similar experiment if monochromatic light is incident on the subject, the scattered light will have the same frequency of the incident light such scattering is known as elastic scattering or Rayleigh scattering. In-elastic scattering of the materials is referred as Raman scattering, during inelastic scattering frequency of scattered light is different from incident light.

Generally, inelastic scattering process accounts molecular vibration in the materials. In inelastic scattering, an emitted photon has a lower energy than incident photon. This energy difference is the energy required to excite a molecule to a higher vibrational mode.
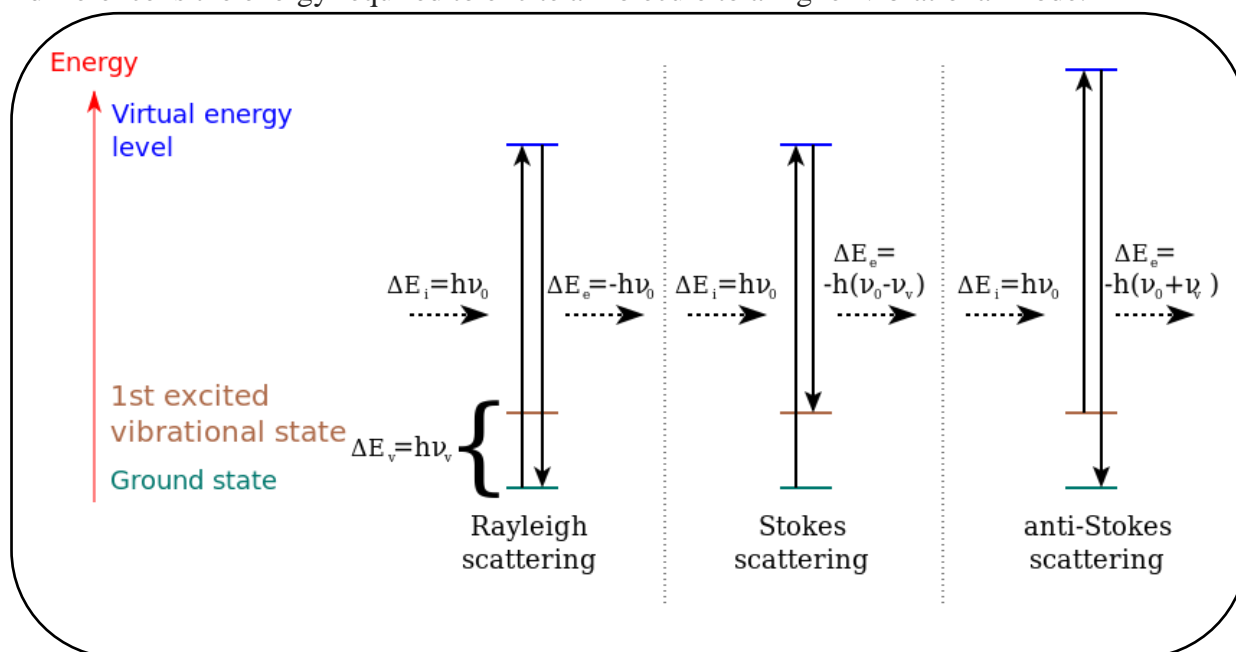
Figure 2.6 Stokes and anti-Stokes scattering in RAMAN Spectroscopy. (Picture Credits: https://en.wikipedia.org/wiki/Raman_scattering)

According to quantum theory of radiation, when photons having energy 'hυ' undergoes elastic collisions with molecules it remains unchanged. A detector placed to collect energy at right angles to an incident beam will thus receive photons of energy 'hυ', i.e. radiation of frequency 'υ'. However, it may happen that energy is replaced between photon and molecule during the collision: such collisions are 'inelastic'. The amount of energy gained or lose by molecule i.e. its energy change (ΔE), must be the difference in energy between two of its allowed states.

Therefore, ΔE is the energy difference between the allowed vibrational and/or rotational transitions of the molecule.

If the molecule gains energy ΔE, the photon will be scattered with the energy hυ-ΔE and the equivalent radiation will have a frequency υ-ΔE/h. Conversely, if the molecule loses energy ΔE, the scattered frequency will be υ+ ΔE/h. Stokes' radiation have frequency lower than that of the incident beam, while that at higher frequencies are called anti-stokes' radiation. Stokes' radiation is generally more intense than anti-Stokes' radiation.

2.4 Fabrication of Li-ion coin cell and Li-ion half coin cell.

Fabrication of lithium ion process is complex process. It involves many steps, machines and chemicals. The details of various steps involving the fabrication is given in this section. Formation of electrode and assembly of cell are the two important main stages of the LIBs manufacturing.

Let us first know the dimension of coin cells.

2.4.1 Dimensions of Coin cell. [72]
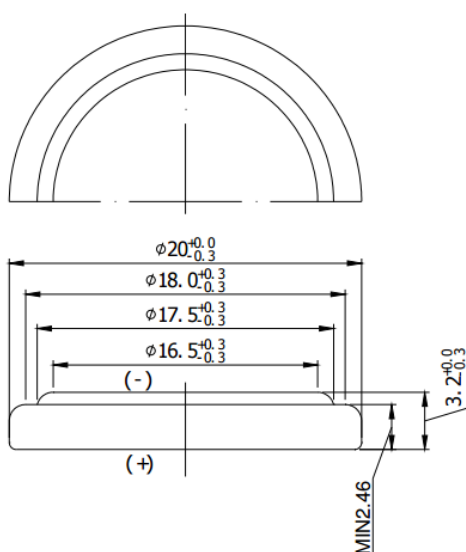
Figure 2.7 Standard dimensions of CR2032 coin cell. *(Picture Credits: http://www.chinabattery.net.cn)*

Nominal Voltage	3V		A	$\varnothing 17.5$
Nominal Capacity	210 (mAh)	Dimensions (mm)	B	$\varnothing 20.0 \, ^{+0.0}_{-0.3}$
Continuous standard load	15 (K Ω)		C	2.46 (Ref.)
Operating temperature	-20~70℃		D	$3.2 \, ^{+0.00}_{-0.30}$
Weight	3.2 (g)			

Figure 2.8 Specification of Li-ion coin cells

2.4.2 Electrode formation process for Li-ion coin cell

2.4.2.1   Cathode Formulation Materials List & Weight Ratios:

I.   Cathode active material (e.g. $LiCoO_2$): 94.5% of main active material that constitutes the positive electrode.

II.   Super-P Conductive Carbon Agent: 1.0% for improving the conductivity of negative electrode.

III.   Carboxymethyl Cellulose (CMC) Thickener: 2.25% for making slurry.

IV.   Styrene-Butadiene Rubber (SBR) Binder: 2.25% for bonding the powders and the aluminium foil or mesh.

V.   De-ionized Water: 120% of active material

VI.   Current Collector Substrate: aluminium foil for electrical contact.

2.4.2.2   Anode Formulation Materials List & Weight Ratios:

I.   Anode active material (e.g. Hard Carbon): 94.5% of main active material that constitutes the negative electrode.

II.   Super-P Conductive Carbon Agent: 1.0% for improving the conductivity of negative electrode.

III.   Carboxymethyl Cellulose (CMC) Thickener: 2.25% for making slurry.

IV.   Styrene-Butadiene Rubber (SBR) Binder: 2.25% for bonding the powders and the copper foil or mesh.

V.   De-ionized Water: 120% of active material.

VI.   Current Collector Substrate: copper foil for electrical contact.

2.4.2.3   Formulation and cutting of electrodes:

Following are the formulation steps involved in the electrode fabrication:

I.   Heat treatment of raw materials: Bake the prepared powders (anode and cathode materials) at 300 ~ 400 °C for an hour under an inert gas atmosphere to remove oily substances from the surface for improving the compatibility with aqueous adhesives. A vacuum oven is recommended for this application.

II.   Milling: Take the active materials and Super-P powders into the jar barrel of a ball type miller/ mixer. Alumina or zirconia balls with diameters <11.5mm and a nylon jar are recommended. About 80% of the jar should be kept empty for the milling clearance. Set a milling speed to at least 60 rpm with duration of 30 minutes to 1 hour. At the end of the milling session, separate the milled powders from the balls by a sieve. (Fig. 2.9)

III. Mixing: With the de-ionized water heated to 80 °C, add and stir the CMC thickening agent until it is fully dissolved in the liquid. Slowly add the SBR binder into the liquid and stir it until full dissolution is attained (add more water if needed). This process could take more than 60 minutes and an automated mixer is recommended. Add in the milled active and conductive powders above with given ratios into the mixed liquid and stir them all together. For achieving the best uniformity, it is recommended to separate the powder into two or more batches and mix them in separate sequences (i.e. add the next batch into the blend once the first batch has been amalgamated). Again, an

Figure 2.9 Ball miller instrument.

automated mixer with a vacuum feature can help eliminate bubbles and yield a homogenous mixture. The slurry is ready for coating on conducting foil.

IV. Viscosity Testing: Test the slurry's viscosity to see if it falls in the range of 5000 and 6000 CPS. Add more de-ionized water if the result is over this range or add more binder and thickener (CMC and SBR) if under.
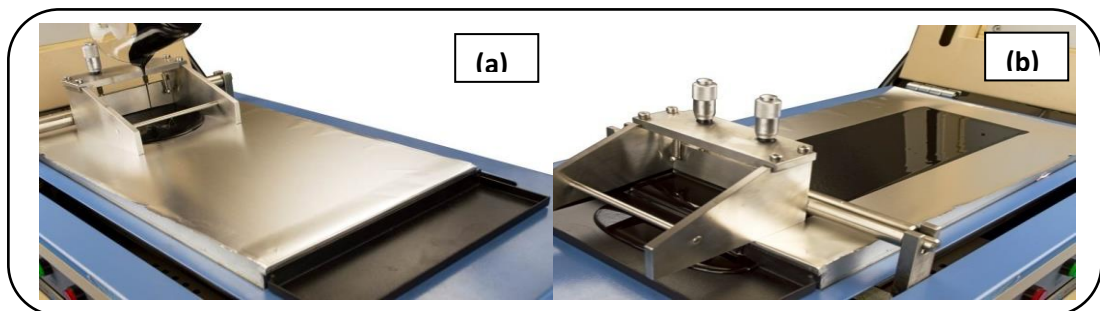
Figure 2.10 Doctor's blade method for coating. (a) Before coating. (b) After coating.

V. Slurry Coating: Sieve the mixed slurry to filter out larger particles from the blend; this ensures the best thickness uniformity on electrode sheets. Use a coating instrument with a Doctor Blade to carry out the coating on a conductive substrate. Wiping the film

substrate with alcohol prior to coating is highly recommended. A heating lid on the coater will help complete this process faster by drying the coating faster. (Fig. 2.10)

VI.   Rolling: Use a rolling calendar to compact the electrode coating for increasing its density. Thickness requirement is at end user's discretion but a 20% to 30% reduction from the original thickness is recommended. (Fig. 2.11)

VII. Cutting: Punch the electrode sheets into round discs (~ 19mm for CR20XX) or strips and Celgard C480 membranes into discs of 19 mm in diameter and use them as separators by using cutting instrument. (Fig. 2.12)

VIII. Drying: Bake the cut electrodes at 110 °C for about 12 hours in a vacuum oven to evaporate out the binder and other chemicals for thoroughly drying the electrodes.

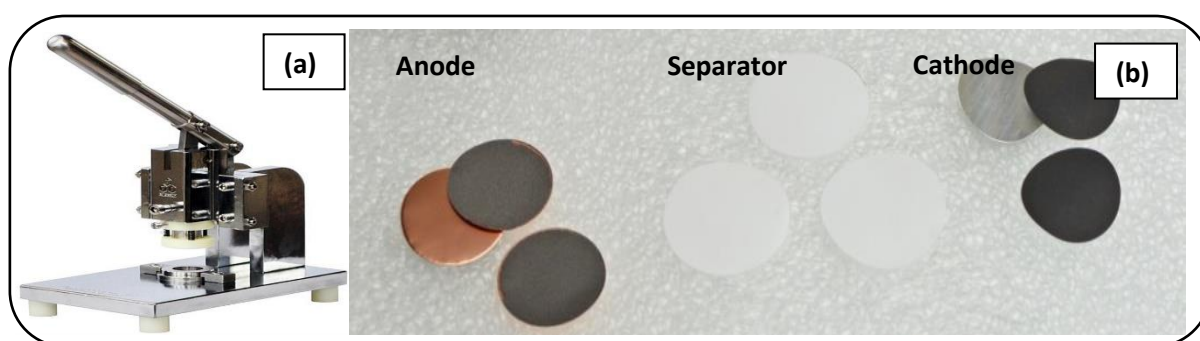*Figure 2.11 Rolling calendar.*

Figure 2.12 (a) Cutting instrument. (b) Cutted pieces of anode, cathode and separator

2.4.3   Assembly of Li-ion half coin cell.

Lithium ion half-cell consist of lithium foil as counter electrode during fabrication of battery. Table 2.1 gives the parameters for additional components used for manufacturing the Li-ion coin cell.

Table 2.1 Material parameters of the components of Li-ion coin cell.

Sr.No.	Components	Material	Dimensions (mm)	Weight (g)
1	Casing	Stainless Steel 304 with sealing O-ring (SS304)	Diameter:20 Height:3.2	3.4019
2	Spring	Stainless Steel	Diameter:14.5(Outer diameter) 10.25(Inner diameter) Height: 0.3(from crest to trough)	2.8350
3	Spacer	Stainless Steel 304(SS304)	Diameter:15.8 Height:0.5	2.8350

Following are the steps involved in assembling the Li-ion half coin cell using prepared MoS_2 materials as working electrode and lithium foil as counter electrode.
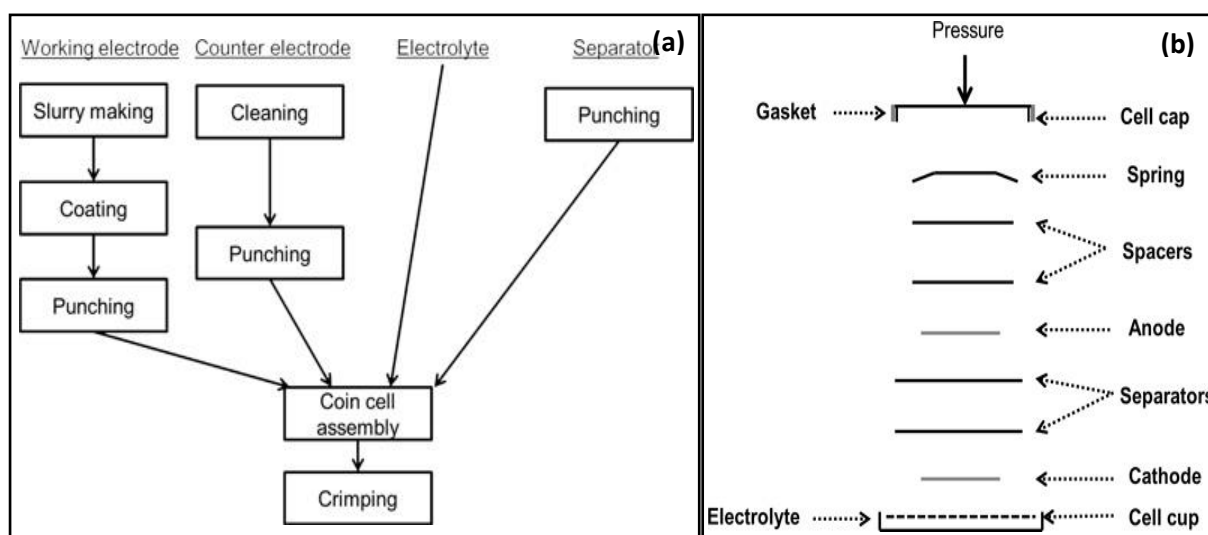
Figure 2.13 (a) Flow chart of the coin cell construction. (b) Schematic of a coin cell assembly including the order of each component in assembly.

I. Fig. 2.13 (a) and (b) shows the flow chart for the coin cell assembly.

II. Inside the glove box transfers the coin cell cases (CR2032), springs and spacers (purchased from MTI Corp.), separators and working electrodes (after flushing the exchanger five times with argon).

III. Assemble the coin cells in the glove box according the steps shown in the shown in Fig. 2.13 (a) and (b).

IV.   At first, take the two drops of the electrolyte on to the cell cup and put the working electrode on it. Take the tree more drops of the electrolyte and put the separators. Add two more drops of the electrolyte before placing the lithium counter electrode on it. Place the two stainless steel spacers and a spring on the lithium disc followed by cell cap.

V.   Finish the cell assembly and crimp cell using the compact crimping machine (purchased from MTI Corp.).

VI.   Avoid the contact between the assembled cell and metals to avoid the short circuit.

VII.   Use the paper napkin to dry the cell from leaking electrolytes.

VIII.   The cell is ready for testing, label it and take it out of the glovebox for electrochemical measurements.

The results and analysis for prepared MoS_2 and nitrogen doped MoS_2 coin cells has been discussed in next chapter including their characterisation results.

2.5   Electrochemical analysis of LIBs.

The capacity, life cycle, specific energy and power can be interpreted from the electrochemical characterisation techniques. The electrochemical performance of fabricated lithium ion battery is tested from following techniques.

2.5.1   Cyclic Voltammetry

Cyclic Voltammetry (CV) is an electrochemical technique that measures the current in an electrochemical cell when voltage is ramped linearly versus time governed by Nernst equation. CV is performed by cycling the potential of a working electrode, and measuring the resulting current.

CV can be used to study qualitative information about electrochemical processes, such as oxidation-reduction of the reactions, the reversibility of a reaction, and to find capacity of the material. The CV is performed at 0.2 mV/s scan rate for potential range 0.01 to 3 V for fabricated lithium ion battery.

2.5.2   Cyclic Charge –Discharge

The cycling life and charge-discharge capacity of battery is performed and calculated from charge – discharge curve. The charge-discharge cycle are performed at the current density of

100 mAh for all fabricated lithium ion coin cell to calculate the capacity of the cell from charge-discharge curve.

2.5.3 Impedance

Impedance is a combined internal resistance and reactance of the battery. The impedance measurements gives the total resistivity of the fabricated coin cell. Lower the impedance higher the performance of battery.

CHAPTER 3: <u>RESULTS AND DISCUSSION</u>

3.1 Synthesis and optimisation of MoS₂ nanostructures.

The optimisation of MoS$_2$ nanostructures is based on expected yield, XRD and FESEM analysis of synthesised MoS$_2$ powder by hydrothermal method. Different parameters were altered to get the optimised product. Table 3.1 gives the synthesis parameters and final yield of the product. All the synthesis were done in 100 ml Teflon container autoclave at 200°C temperature. The expected yield of the reaction is calculated from initial and final moles molybdenum atom present in reaction. The expected yield for MoS$_2$ is around 0.8035 grams when 0.8828 grams of molybdenum precursor taken for synthesis i.e. one mole of molybdenum.

Table 3.1 Synthesis parameters for optimisation MoS$_2$ nanostructures.

Sample Name	Mo:S ratio in precursor	Water (ml)	Time (hrs)	Yield (g)
CK-1	1:2.5	30	24	0.6587
CK-2	1:2.5 (different precursor)	30	24	1.19149
CK-3	1:2.5	30	12	0.5352
CK-4	1:2.5	30	6	0.3997
CK-5	1:2.5	30	3	0.1104
CK-6	1:2.5	30	48	0.4103
CK-7	1:2.5	30	72	**0.8097**
CK-8	1:2.5	60	24	0.2993
CK-9	1:4	30	24	0.5539
CK-10	1:8	30	24	0.7928
CK-11 (optimised)	1:8	60	24	**0.8425**
			Expected Yield	**~0.8035**

3.1.1   XRD and expected yield analysis

First, we started with two sulphur precursor (thiourea for CK-1 and thioacetamide for CK-2), yield of CK-2 is more than expected and XRD pattern of CK-2 powder does not contained the (002) peak around $2\theta = 14°$. Thus, we finalised thiourea as sulphur precursor for synthesis of MoS_2 as XRD pattern of CK-1 is matching with hexagonal semiconducting phase (Fig. 3.1). Then we varied the duration of reaction from 3 hrs to 72 hrs (CK-3 to CK-7) and noticed that at longer duration expected yield is achieving as molybdenum precursor is completely transforming into the product. To reduce the duration for reaction, we increased the
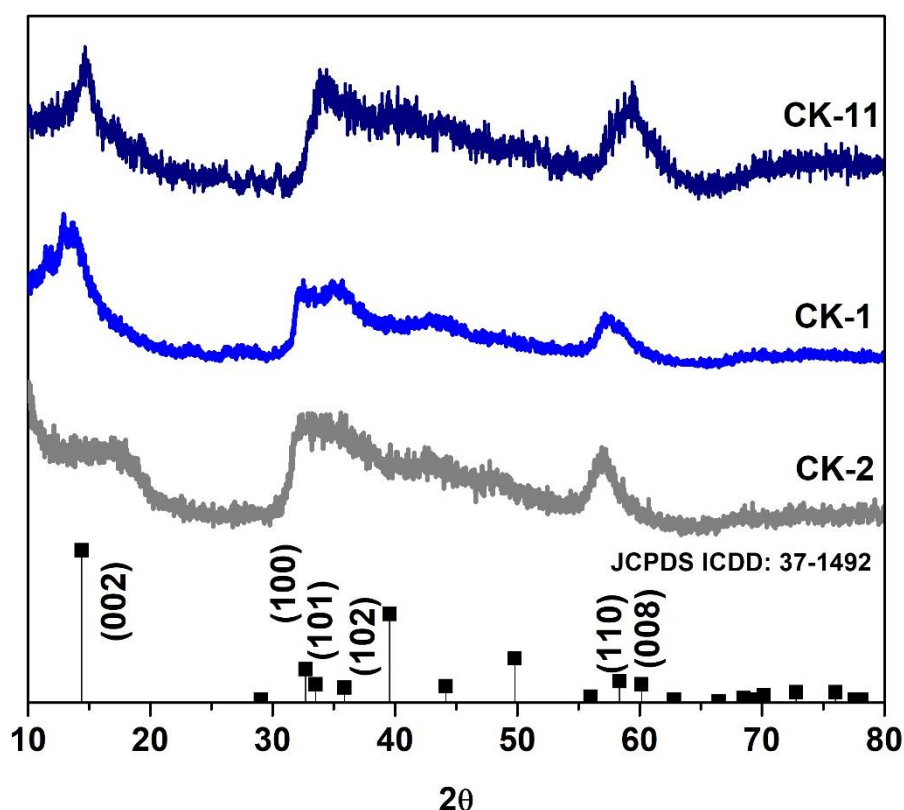

Figure 3.1 X-ray diffraction pattern for CK-1, CK-2, CK-11, and JCPDS for 2-H MoS₂

concentration of sulphur precursor and pressure (increasing the solvent), and finally optimised (CK-11) the MoS_2 nanostructures powder. The XRD pattern of CK-3 to CK-11 are matching with the XRD pattern of CK-11.

The XRD pattern of optimised CK-11 is matches with standard MoS_2 pattern (JCPDS ICDD No. 37-1492). The intense and broad reflection peaks confirms the formation MoS_2 nanostructure. The observed XRD reflection peaks at $2\theta = 14.53°$, $32.67°$, $33.50°$, $32.87°$, $39.53°$, $58.33°$, and 60.14 corresponds to (002), (100), (101), (102), (103), (110), and (008) respectively. The alternation in reaction time does not show any appreciable changes in peak

height and position. Overall XRD pattern confirms the formation of nanocrystalline hexagonal semiconducting phase of MoS_2 prepared by hydrothermal route method.

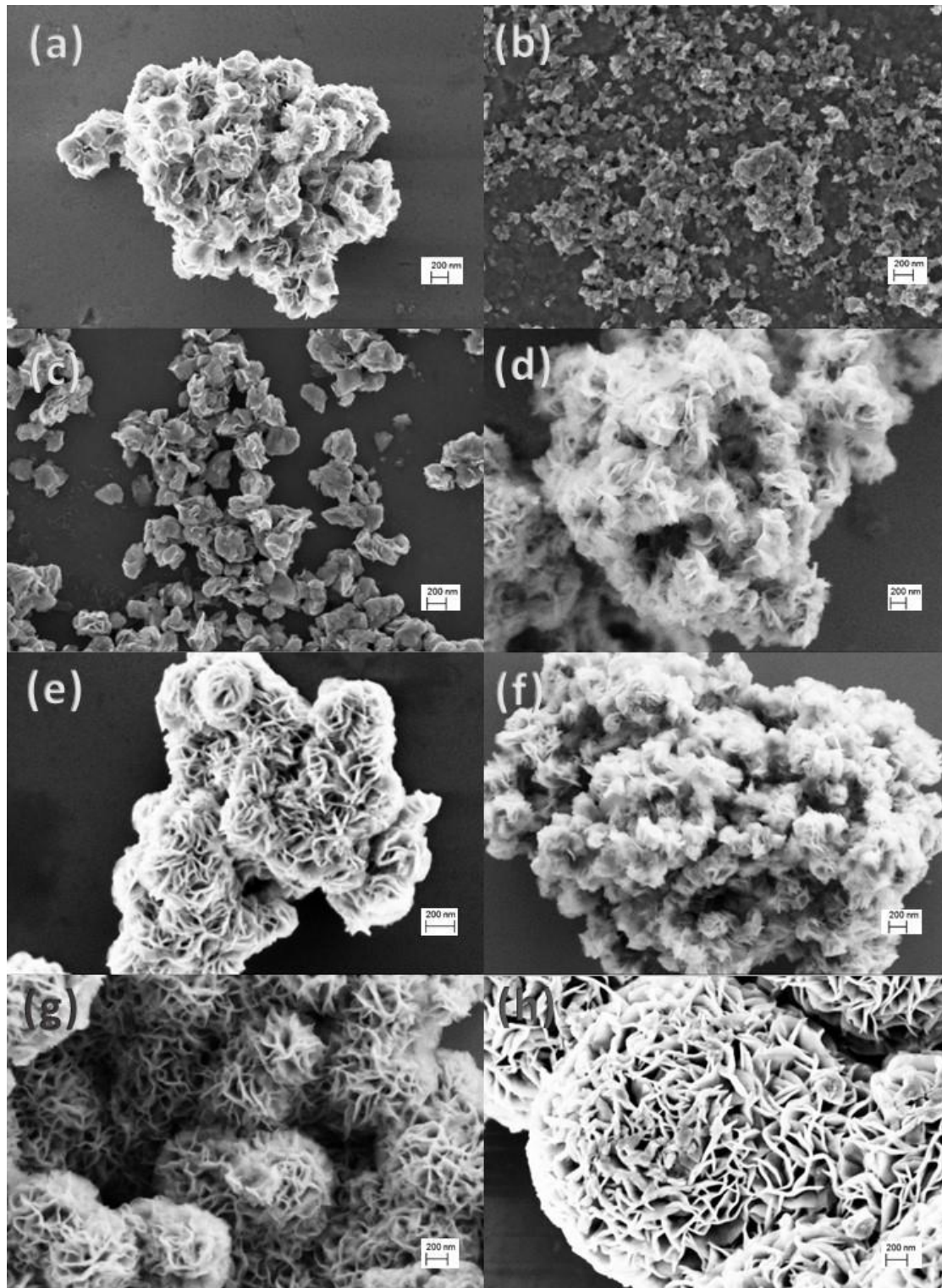### 3.1.2 FESEM analysis for optimisation of MoS_2 nanostructures

Figure 3.2 FESEM images of (a) CK-1, (b) CK-2, (c) CK-3, (d) CK-7, (e) CK-8, (f) CK-9, (g) CK-10, and (h) CK-11.

Along with XRD, FESEM helped to optimise the MoS$_2$ nanostructures. The variation in synthesis procedure reflected in the morphology of synthesised materials. Figure 3.2 shows the surface morphology of synthesised MoS$_2$ nanostructures during optimisation process. The FESEM characterisation confirms the formation of flowerlike structure of MoS$_2$ nanosheets.

The formation flower like structure is not observed in the case of CK-2 (Fig. 3.2 (b)). The optimisation process leads to formation more structured flowers with high surface nanosheets. The figure 3.2 (a) – (h) shows the surface structure of CK-1, CK-2, CK-3, CK-7, CK-8, CK-9, CK-10, and CK-11 respectively. The effect of duration on the growth of the nanosheets can be seen between Fig. 3.2 (a) and (d). The effect of pressure on the morphology of material can be seen in Fig. (a) and (e). The morphology comparison between the Fig. 3.2 (a), (f) and (g) confirms the effect of concentration during the optimisation process. Thus, final optimised MoS$_2$ nanostructures can be seen in Fig. 3.2 (h). The optimised MoS$_2$ i.e. CK-11 is synthesised at 200˚C in 60 ml of water with Mo:S mole ratio of 1:8 for 24 hrs in hydrothermal. The CK-11 is termed as MoS$_2$ for further analysis and application.

3.2 Synthesis of Nitrogen doped MoS₂ nanostructures.

The nitrogen doped MoS_2 nanostructures were characterised by different techniques to study the effect of doping on optical, physical and chemical properties of MoS_2 nanosheets.

3.2.1   XRD analysis

The XRD pattern of nitrogen doped MoS_2 nanostructures (MoS_2 400, MoS_2 N1, MoS_2 N3 and MoS_2 N5) is compared with XRD pattern of optimised MoS_2 (CK-11) in figure 3.3. After nitrogen doping in MoS_2 there is slight change in XRD peak intensity but position of peak remained same. The broadening of the XRD peak is decreased indicating more crystalline structure of nitrogen doped MoS_2. From the XRD it is confirmed that MoS_2 materials are in nanoscale after nitrogen doping. Two new peaks are observed in case MoS_2 N1 at $2\theta = 26.74°$ and 54.33°. Other than that, XRD results are as expected and further analysis is done for confirming the same.
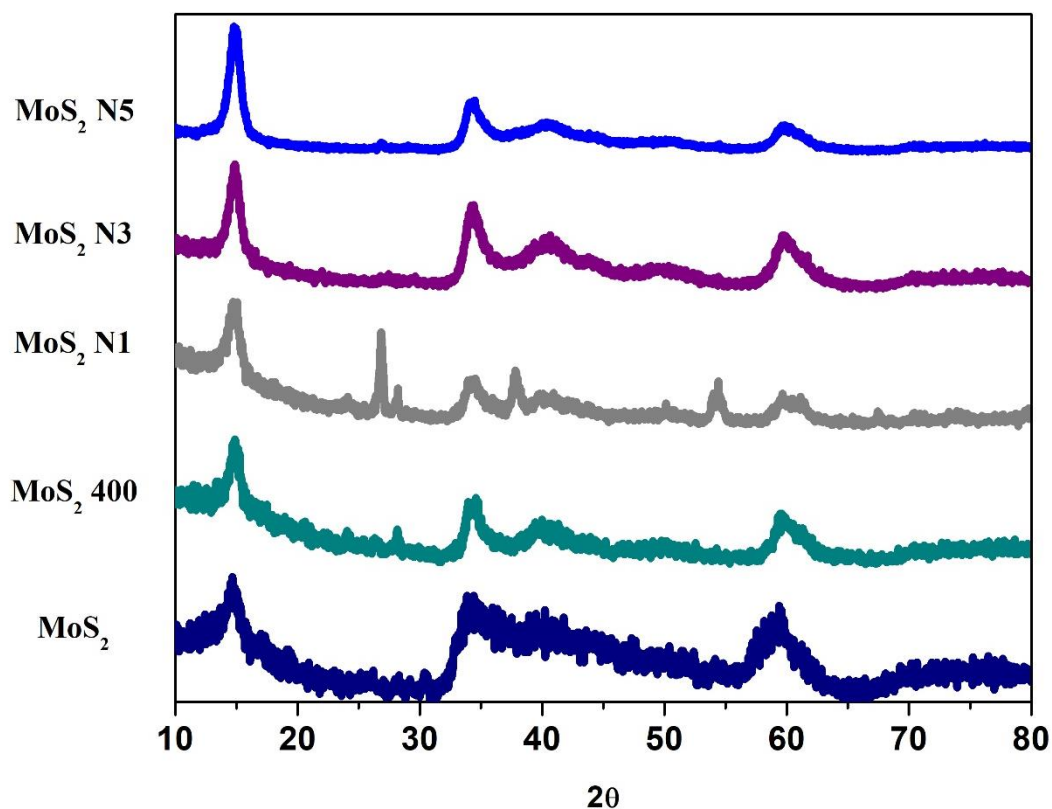

Figure 3.3 XRD pattern for prepared MoS₂, MoS₂ 400, MoS₂ N1, MoS₂ N3, and MoS₂ N5.

3.2.2 Diffuse reflectance UV-Visible spectroscopy.

To study the optical properties of synthesised materials diffuse reflectance UV-Visible spectra is recorded in the range from 200 nm to 800 nm of doped and as synthesised MoS_2
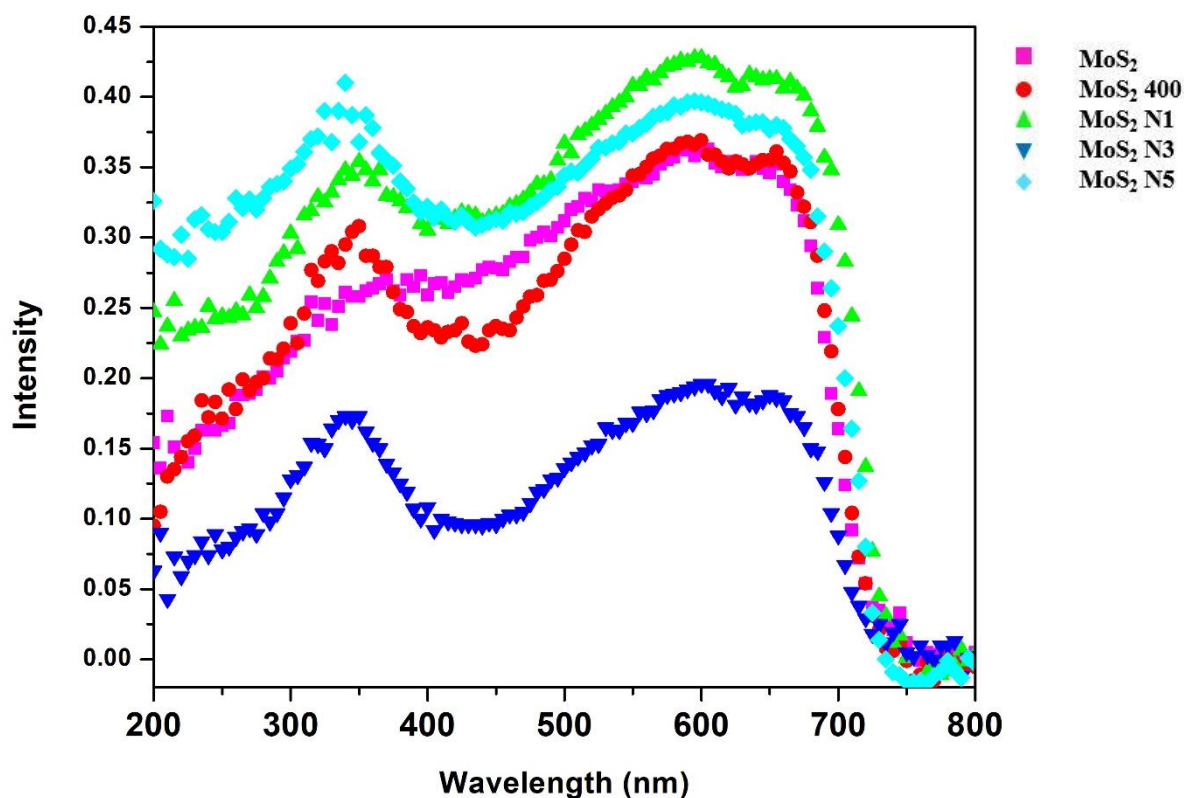

Figure 3.4 Diffuse reflectance UV-Visible absorbance spectra of MoS₂, MoS₂ 400, MoS₂ N1, MoS₂ N3 and MoS₂ N5.

nanomaterials. The as synthesised MoS_2 showed the single broad absorption peak while two broad peaks are observed in nitrogen doped MoS_2 nanostructures. This indicates the change in band gap structure and successful doping of nitrogen in MoS_2 nanosheets. FESEM analysis is done to study surface morphology and id discussed in next section (3.2.3).

3.2.3 FESEM analysis of nitrogen doped MoS₂ nanostructure.

The FESEM images shows the surface and morphological differences between the MoS_2, MoS_2 400, MoS_2 N1, MoS_2 N3, and MoS_2 N5 nanostructures. MoS_2 400 shows the growth in nanosheets than the as synthesised MoS_2 (Fig. 3.5 (a-d)). Thus, more intense peak in XRD pattern. Heating as synthesised MoS_2 at 400˚C with urea modifies the nanosheets in flower like structure and confirms the structural integration of nitrogen with MoS_2. As we see in the figure 3.5 (e-f), increase in nitrogen doping in MoS_2 breaches more the nanosheets. In figure 3.5 lower and higher magnification images of MoS_2, MoS_2 400, MoS_2 N1, MoS_2 N3, and MoS_2 N5

nanostructures has been shown. The surface structure of MoS_2, MoS_2 400, MoS_2 N1, MoS_2 N3, and MoS_2 N5 nanostructures is as expected and is consistent with the other characterisation results. From FESEM size of the each petal in flower is between 20-50 nm. To know more about structural and morphological details TEM analysis of prepared nanostructure is done and discussed in next section (3.2.4).
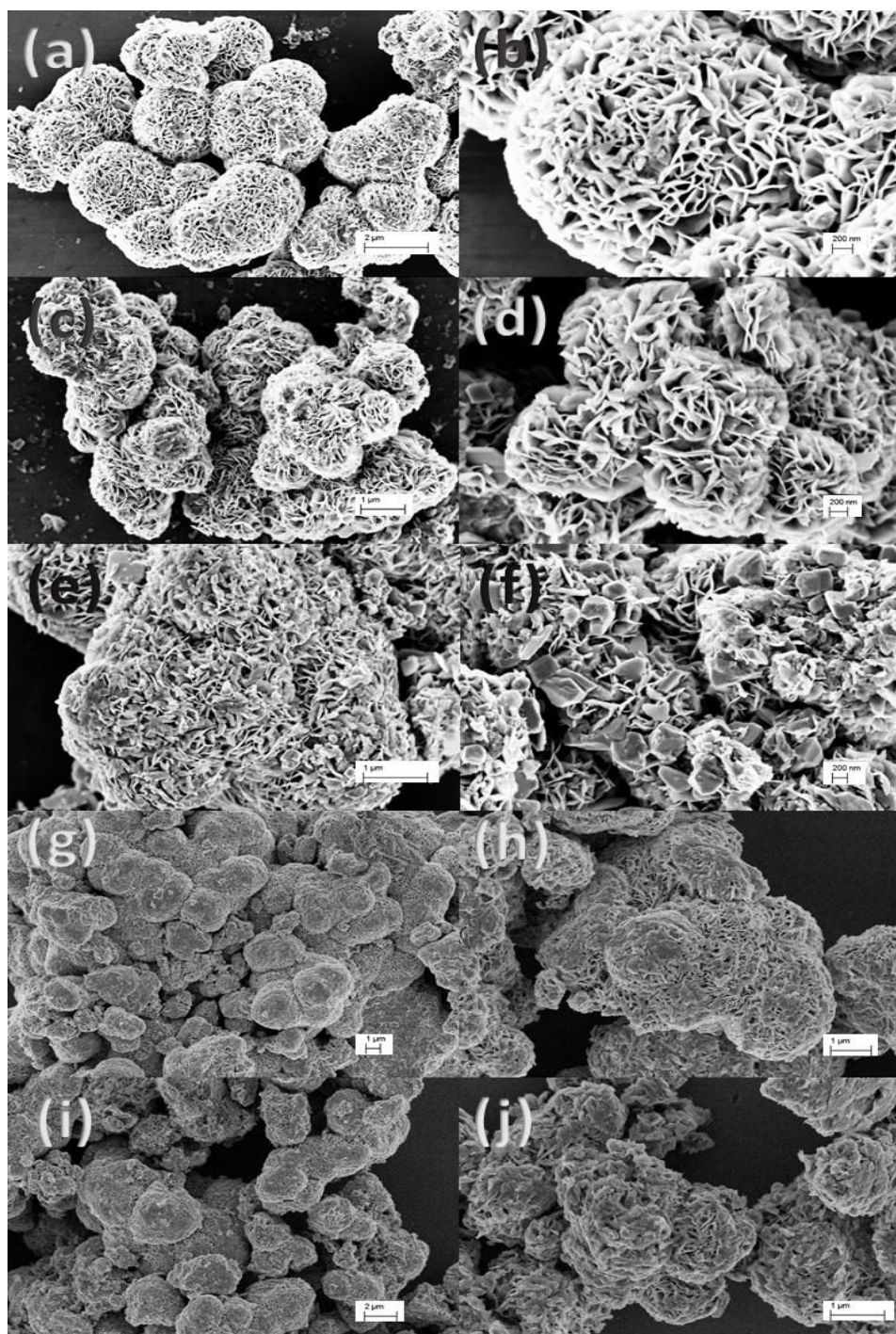

Figure 3.5 Lower and higher magnification FESEM images of (a, b) MoS₂, (c, d) MoS₂ 400, (e, f) MoS₂ N1, (g, h) MoS₂ N3 and (I, j) MoS₂ N5 nanostructures.

3.2.4 TEM analysis of nitrogen doped MoS₂.

The microstructural analysis of prepared MoS₂ nanomaterials was studied using TEM analysis and images. The figure 3.6 shows the TEM images of (a, and b) MoS₂, (c, and d) MoS₂ 400 and (e, and f) MoS₂ N1. TEM analysis clearly indicates the formation of flower like morphology consist of stacked nanosheets as flower petals. The growth of petals of MoS₂ flower can be seen in the Fig. 3.6 (a and c). As discussed in FESEM analysis (section 3.2.3), nitrogen doping in MoS₂ leads the rupturing of nanosheets in flowers which can be easily seen in the TEM images in Fig. 3.6 (c, and e). The size of petals in as synthesised MoS₂ is between 20 -50 nm, for MoS₂ 400 is between 20 – 80 nm. However, for MoS₂ N1 petal size decreased to 20 – 40 nm due to nitrogen doping. Every petal is formed by staking of 20-80 two-dimensional MoS₂ nanosheets and can be easily seen in figure 3.6 (b, d, and f). The layered structure of prepared MoS₂ is confirmed from TEM analysis.
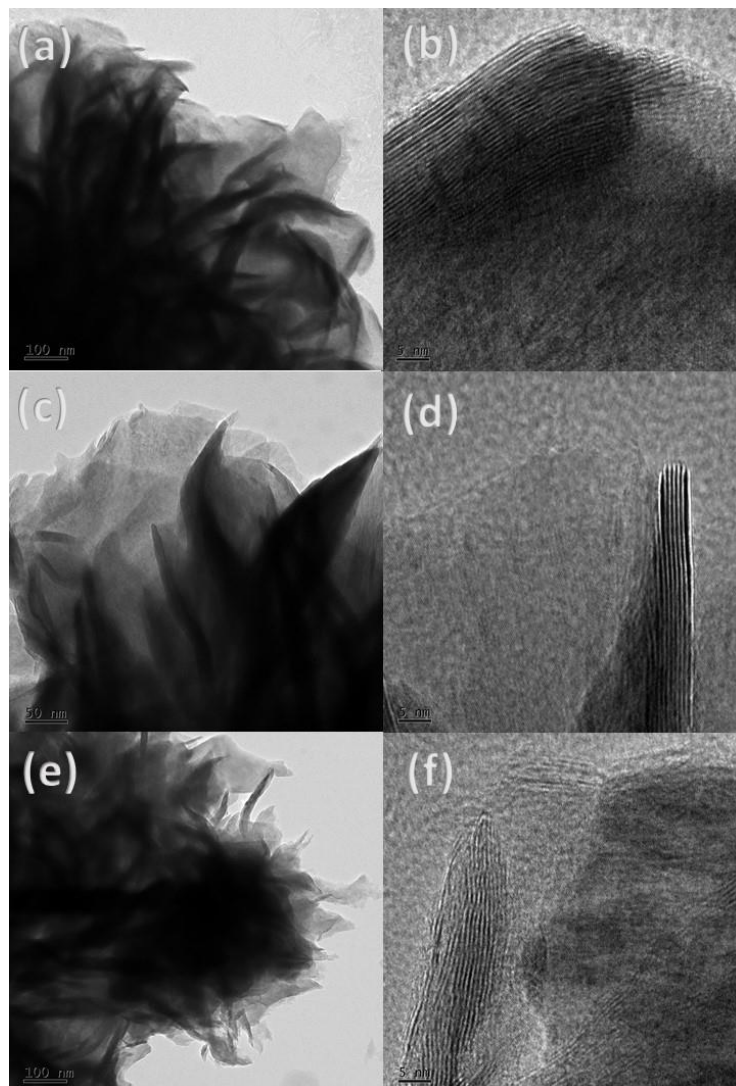

Figure 3.6 TEM images of (a, b) MoS₂, (c-d) MoS₂ 400 and (e-f) MoS₂ N1

The crystal structure analysis of prepared MoS_2 nanomaterials were studied using the fringes and SAED pattern in TEM analysis. The figure 3.7 (a-d) shows the fringes and SAED pattern of MoS_2 N3 and MoS_2 N5. The figure 3.7 (a, and c) shows the different crystallographic planes and inter planer distance of MoS_2 N3 and MoS_2 N5 respectively. The inter planer distance is exactly matching with those calculated from XRD pattern. The SAED pattern has shown the intense pattern at respected d-spacing value. Figure 3.7 (b) shows the ring pattern for MoS_2 N3 while figure 3.7 (d) shows the dotted pattern for MoS_2 N5. The hkl planes in SAED pattern of MoS_2 N5 is marked in Fig. 3.7 (d). The hkl planes and their d-spacing is exactly matching with those calculated from XRD pattern. Thus, TEM analysis shows the consistent results with XRD results. Overall TEM images and SAED patterns confirms the formation of crystalline hexagonal phase in prepared MoS_2.
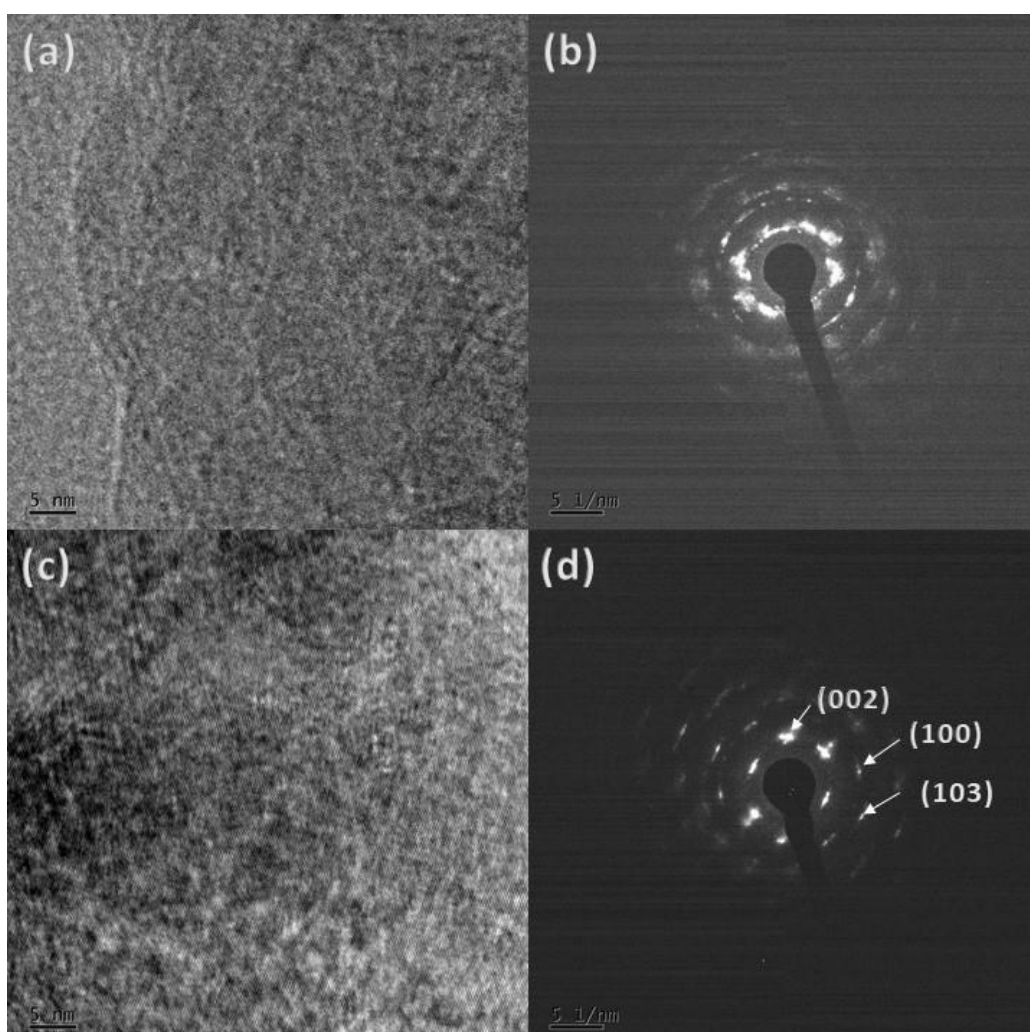

Figure 3.7 Fringes and SAED pattern of (a, and b) MoS2 N3 and (c, and d) MoS2 N5.

3.2.5 BET surface area measurements

The specific surface area of a prepared MoS_2 nanomaterial is analysed by BET surface area analyser. The BET theory accounts for the physical adsorption of gas on a surface. It is an important analysis technique for measuring the specific surface area of a material. The table 3.2 shows the specific surface area calculated from the BET analyser of prepared MoS_2 nanomaterials.

Table 3.2 BET surface area measurements of MoS_2, MoS_2 400, MoS_2 N1, MoS_2 N3, and MoS_2 N5.

Sample Name	Surface area (cm^2/g)
MoS_2	7.8
MoS_2 400	15.0
MoS_2 N1	14.1
MoS_2 N3	5.5
MoS_2 N5	6.2

The specific surface area has increased from 7.8 to 15.0 cm^2/g, which confirms the growth in surface area in MoS_2 400 than MoS_2. The specific surface area has decrease in MoS_2 nanomaterials as nitrogen doping is increased. The BET surface area measurements are consistent with FESEM and TEM results.

3.2.6 Hall measurements

The conductivity study of the prepared MoS_2 nanomaterials is done by the hall effect measurement. The Hall Effect measurement were studied on MoS_2, MoS_2 400, and MoS_2 N1 materials. The MoS_2 is found to be as n-type of semiconductor with average hall coefficient of -5.7361E+05 and bulk conductivity of -1.1637E+13. The nitrogen doped MoS_2 400 and MoS_2 N1 is found to be p-type of semiconductor with average hall coefficient is 4.5588E+05 and

2.4536E+05 respectively. This confirms the successful nitrogen doping and enhancement in conductivity of the MoS_2 nanomaterials.

3.2.7 Raman analysis

The structure of MoS_2 and nitrogen doped MoS_2 are analysed with Raman spectroscopy technique. Figure 3.8 shows the Raman peaks for synthesised MoS_2 nanomaterials. The two peaks corresponds to E^1_{2g} and A_{1g} vibrations at 377 and 403 cm^{-1} for prepared MoS_2 respectively. These two Raman peaks are consistent with literature values. The nature of nitrogen doped MoS_2 Raman peaks matches with as synthesised MoS_2. The nitrogen doped MoS_2 shows the blue shift as compared with pristine MoS_2 Raman peaks along with broadening of the Raman peaks. The Raman analysis confirms the structural changes after the nitrogen doping in MoS_2.
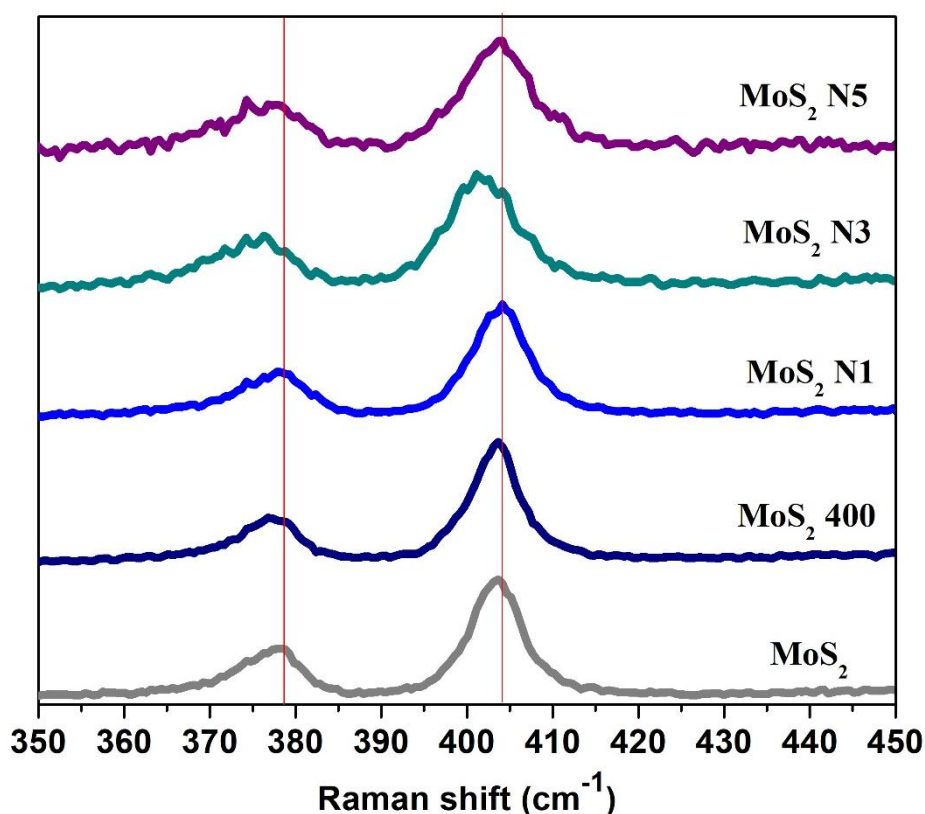
Figure 3.8 Raman scattering peaks for MoS$_2$, MoS$_2$ 400, MoS2 N1, MoS2 N3 and MoS2 N5.

3.2.8 Electrochemical analysis of fabricated lithium ion half-cell.

The electrochemical characterisation were done on lithium ion coin half-cell using prepared MoS_2 as anode material. The figure 3.9 (a-c) shows the Cyclic Voltammetry (CV) curves for MoS_2, MoS_2 N3, and MoS_2 400 at 0.2 mV/s scan rate respectively. The MoS_2 and MoS_2 400

coin cell showed the good cyclic behaviour in CV curve, hence proceeded for further analysis. Nitrogen doped MoS_2 N3 have lesser cyclic repeatability. The Fig. 3.9 (d) shows the characteristic impedance curve of MoS_2 400 before and after CV. Lithium ion coin half-cell using MoS_2 400 anode has shown the best performance.
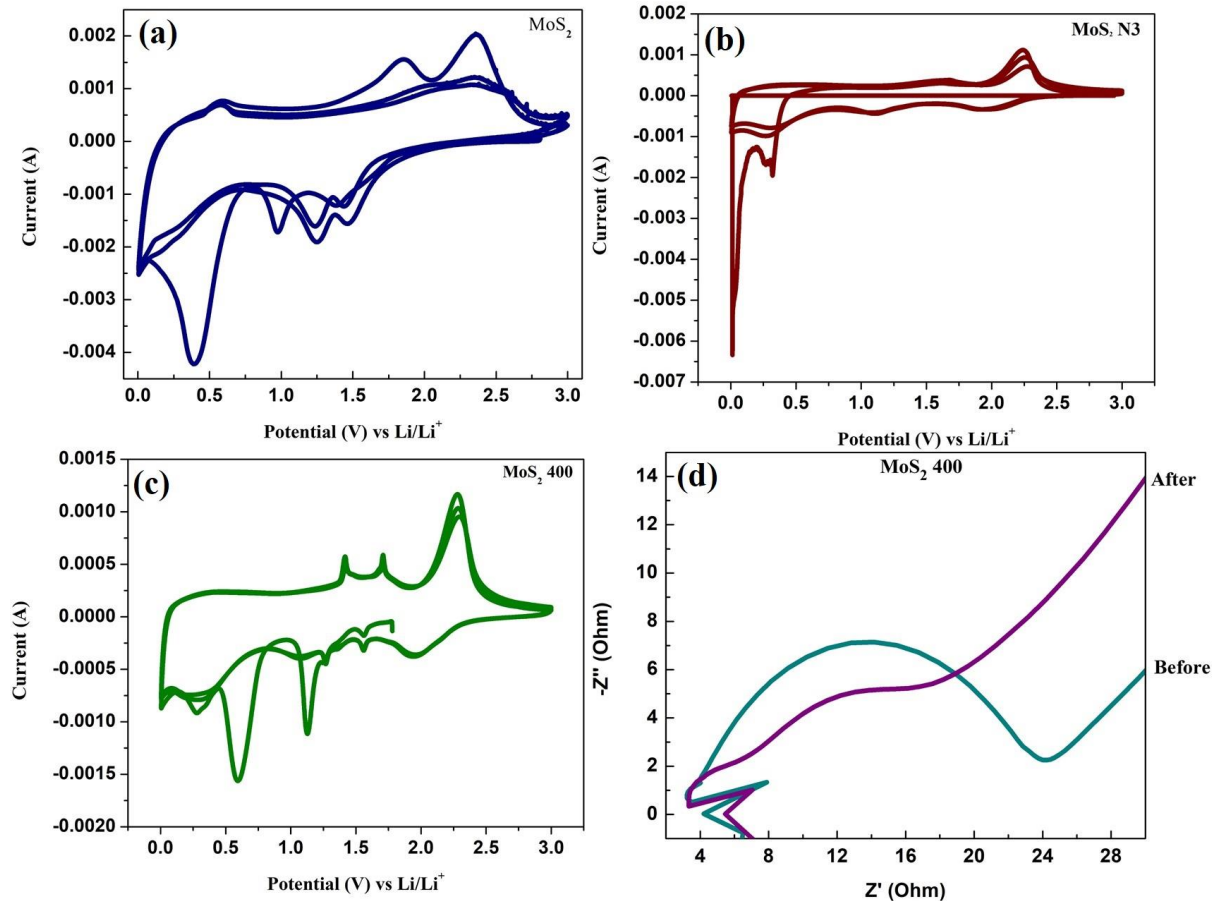
Figure 3.9 Cyclic Voltammetry curve for (a) MoS₂, (b) MoS₂ N3, and (c) MoS₂ 400. (d) Impedance curve for MoS₂ 400.

The cyclic charge-discharge of fabricated coin cell is done to check their capacity and capacity fading. The figure 3.10 (a and b) shows the charge discharge curve for MoS_2 and MoS_2 400 for first 15 cycles respectively. In Fig. 3.10 (c and d) the specific capacity during charging and discharging for first 15 cycles is given. The efficiency of each cycle is also plotted as function of cycle number in the same plot. The initial values for efficiency are near around 100%, however efficiency decreases as number of cycles increase. The capacity fading is seen as number of cycles increases. Table 3.3 gives the value of capacitance up to three cycles.

Table 3.3 Charge-Discharge capacitance of MoS₂ and MoS₂ 400.

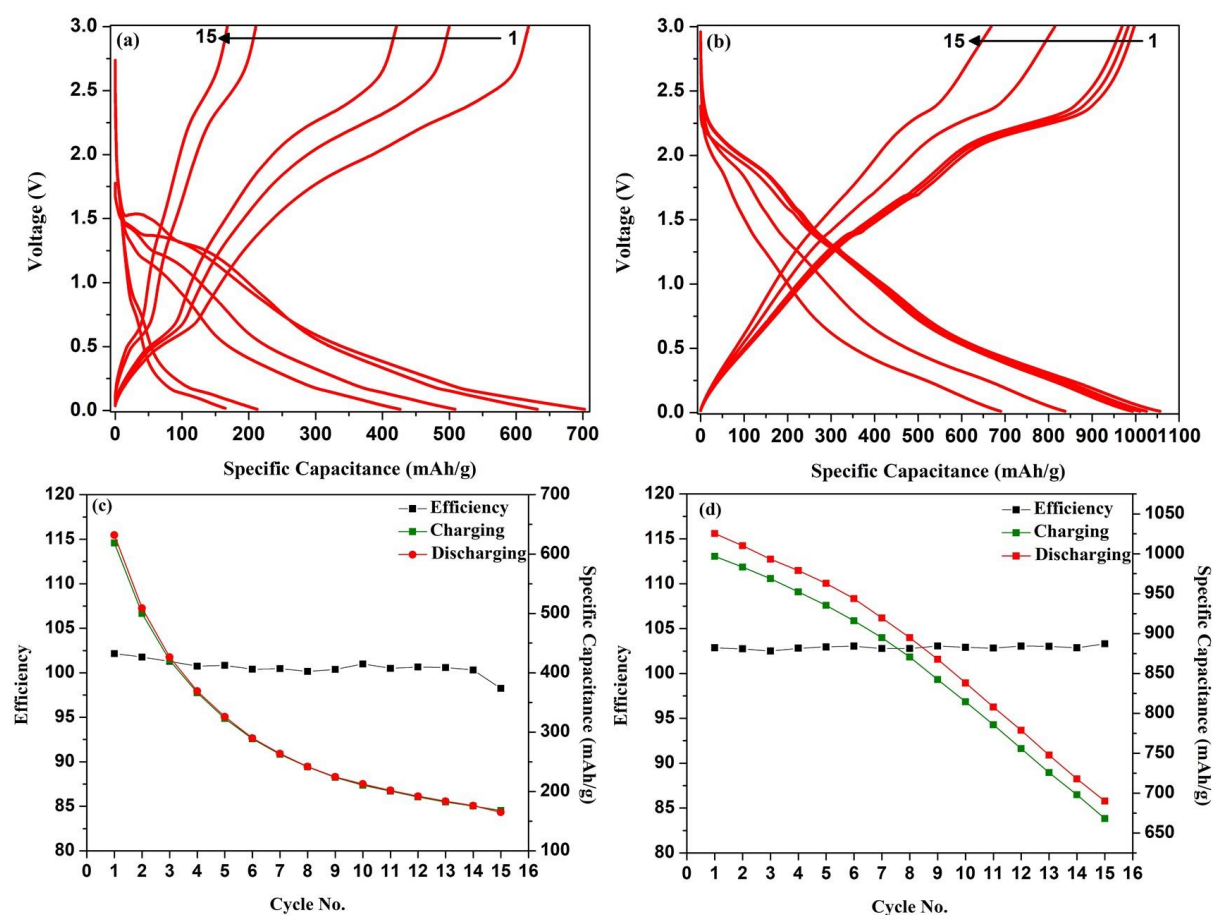| Cycle no.	Charging Capacity	Discharging Capacity	Efficiency	Anode material
1	618.7003	632.043	102.15	MoS₂
2	499.9709	508.8284	101.77	MoS₂
3	421.0391	426.4129	101.28	MoS₂
1	996.8273	1025.2904	102.85	MoS₂ 400
2	983.145	1010.1047	102.74	MoS₂ 400
3	968.8818	993.1486	102.5	MoS₂ 400

Figure 3.10 Charge discharge curve for MoS₂ and MoS₂ 400 lithium ion coin half-cells.

The figure 3.11 shows the fabricated lithium ion coin cell using MoS_2 nanomaterials as anode at C-MET Pune.
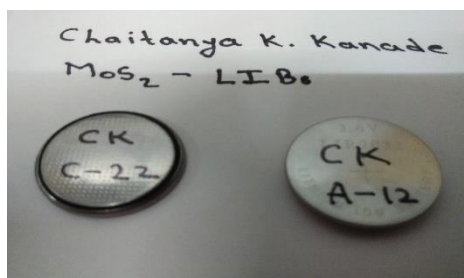
Figure 3.11 Lithium ion coin cell fabricated at C-MET, Pune using prepared MoS2 nanomaterials.

3.3 Summary

The hexagonal semiconducting MoS_2 nanostructures were successfully synthesised the by the hydrothermal route method. The nitrogen doping in MoS_2 is reported first time and confirmed by many characterisation techniques. The formation of hexagonal phase is confirmed by XRD and TEM analysis. FESEM and TEM shows the flower like morphology of the prepared MoS_2 nanomaterials. The each petal of flower is formed by staking of MoS_2 nanosheets and have size in the range of 20-80 nm. The effect of nitrogen doping on optical, chemical, structural properties of MoS_2 is studied by UV-Visible spectroscopy, FESEM, TEM, XRD, Raman spectroscopy etc. The lithium ion coin cell is fabricated using prepared MoS_2 nanomaterials as anode material and tested for their capacity and cycle life. The MoS_2 400 nanomaterial has shown the capacitance of up to 996 mAhg^{-1} in fabricated lithium ion coin cell.

CHAPTER 4: <u>CONCLUSTION</u>

4.1 Conclusion

Concisely, the hexagonal semiconducting MoS_2 nanomaterials is synthesized using hydrothermal method. The first time nitrogen doping in MoS_2 is reported and confirmed by many characterisation techniques. Many characterisation techniques are used to study the effect of nitrogen doping on optical, chemical, physical, and electrical properties of synthesised MoS_2. XRD, TEM, and Raman have been used to investigate the phase purity of prepared MoS_2 anode materials. The further morphological study has been performed by FESEM and TEM, which shows flower like morphology of prepared MoS_2 nanostructures. The petals of MoS_2 flowers are formed by staking of nanosheets and are in the range of 20 - 80 nm. The nitrogen doped MoS_2 showed the enhanced optical and electrical properties than pristine MoS_2. The MoS_2 nanostructures were used as anode materials to fabricate the lithium ion batteries. The lithium half cells of diameter 20mm size have been fabricated using our anode electrodes and showed the specific capacitance up to 996 $mAhg^{-1}$ for MoS_2 400 nanostructure. The electrochemical performance of these cells was studied and they showed excellent charge capacity. There is a good enhancement in capacity due to materials nanocrystalline nature of MoS_2. The research will be continued for much better capacity for miniaturization of the cell.

4.2 Future Scope

The synthesised materials will be used for enhancement of solar cell applications and other optical applications.

- The composite of nitrogen doped graphene and nitrogen doped MoS_2 can show the promising results in energy storage application such as lithium ion battery and sodium ion batteries.
- The MoS_2 nanostructures can be used as electrode for supercapacitor application.
- MoS_2 is well known photocatalyst, hence can be used in applications like solar cell, water splitting for hydrogen generation. The band gap present in MoS_2 can be tuned by doping for more photocatalytic applications.
- MoS_2 is an important component of electronic devices as transistor. MoS_2 transistors can be prepared using prepared MoS_2 nanomaterials.
- MoS_2 can be used as complete energy harvesting material for green chemistry applications.
- WS_2 is allied to MoS_2, similar work can be done with WS_2.

References:

1. Masaki Yoshio, Ralph J. Brodd, Akiya Kozawa, *Lithium-ion Batteries: Science and Technology*, 2009 Ed., Springer.

2. M. Armand, J.M. Tarascon, *Nature* 451 (2008) 652-657.

3. G.P. Gholam, Abbas Nazri, *Lithium Batteries: Science and Technology*, 2003 ed., Springer.

4. M. Winter, R.J. Brodd, *Chem. Rev.* 104 (2004) 4245-4270

5. J.M. Tarascon, M. Armand, *Nature* 414 (2001) 359-367.

6. B. Xu, D. Qian, Z. Wang, Y.S. Meng, *Mater. Sci. Eng.: R: Rep.* 73 (2012) 51-65.

7. A.K. Shukla and T.P. Kumar, *Curr. Sci.*, 94 (3) (2008), pp. 314–331.

8. H.A. Kiehne, editor, *Battery Technology Handbook*, 2nd edition, (New York: Marcel Dekker, Inc., 2003).

9. J. Besenhard, editor, *Handbook of Battery Materials* (Weinheim, Germany: Wiley-VCH, 1999).

10. Younesi, Reza; Veith, Gabriel M.; Johansson, Patrik; Edström, Kristina; Vegge, Tejs, *Energy Environ.Sci.* 2015, 8 (7): 1905–1922.

11. J. Newman and C. Monroe, *J. Electrochem. Soc.* 152 (2) (2005), pp. A396–A404.

12. Can, Cao; Zhuo-Bin, Li; Xiao-Liang, Wang (2014), *Frontiers in Energy Research*. 2: 2–8.

13. M. Ge, J. Rong, X. Fang, C. Zhou, *Nano Lett*. 12 (2012) 2318-2323.

14. B.J. Landi, M.J. Ganter, C.D. Cress, R.A. DiLeo, R.P. Raffaelle, *Energy Environ. Sci.* 2 (2009) 638-654.

15. C. Kim, K.S. Yang, M. Kojima, K. Yoshida, Y.J. Kim, Y.A. Kim, M. Endo, *Adv. Funct. Mater.* 16 (2006) 2393-2397.

16. J. Hou, Y. Shao, M.W. Ellis, R.B. Moore, B. Yi, Phys. *Chem. Chem. Phys.* 13 (2011) 15384-15402.

17. H. Zhou, S. Zhu, M. Hibino, I. Honma, M. Ichihara, *Adv. Mater*. 15 (2003) 2107-2111.

18. J. Yang, Y. Takeda, N. Imanishi, C. Capiglia, J.Y. Xie, O. Yamamoto, *Solid State Ionics* 152-153 (2002) 125-129.

19. I.-S. Hwang, J.-C. Kim, S.-D. Seo, S. Lee, J.-H. Lee, D.-W. Kim, *Chem. Commun.* 48 (2012) 7061-7063.

20. K. Zhuo, M.-G. Jeong, C.-H. Chung, *J. Power Sources* 244 (2013) 601-605.

21. J. Jiang, Y. Li, J. Liu, X. Huang, C. Yuan, X.W. Lou, *Adv. Mater.* 24 (2012) 5166-5180.

22. Z. Wang, L. Zhou, X.W. Lou, *Adv. Mater.* 24 (2012) 1903-1911.

23. P.P. Prosini, M. Carewska, S. Loreti, C. Minarini, S. Passerini, *Int. J. Inorg. Mater.* 2 (2000) 365-370.

24. C.-H. Lai, M.-Y. Lu, L.-J. Chen, *J. Mater. Chem.* 22 (2012) 19-30.

25. S. Boyanov, K. Annou, C. Villevieille, M. Pelosi, D. Zitoun, L. Monconduit, *Ionics* 14 (2008) 183-190.

26. L. Ji, Z. Lin, M. Alcoutlabi, X. Zhang, *Energy Environ. Sci.* 4 (2011) 2682-2699.

27. Q. Sun, X.-Q. Zhang, F. Han, W.-C. Li, A.-H. Lu, *J. Mater. Chem.* 22 (2012) 17049-17054.

28. A. Ueda, M. Nagao, A. Inoue, A. Hayashi, Y. Seino, T. Ota, M. Tatsumisago, J. *Power Sources* 244 (2013) 597-600.

29. H. Hwang, H. Kim, J. Cho, *Nano Lett.* 11 (2011) 4826-4830.

30. J. Chen, X.-h. Xia, J.-p. Tu, Q.-q. Xiong, Y.-X. Yu, X.-l. Wang, C.-d. Gu, *J. Mater. Chem.* 22 (2012) 15056-15061.

31. P.G. Bruce, B. Scrosati, J.-M. Tarascon, Angew. *Chem. Int. Ed.* 47 (2008) 2930-2946.

32. Y. Wang, H. Li, P. He, E. Hosono, H. Zhou, *Nanoscale* 2 (2010) 1294-1305.

33. Nahong Zhao, Lijun Fu, Lichun Yang, Tao Zhang, Gaojun Wang, Y. Wu, a.T.v. Ree, *Pure Appl. Chem.* 80 (2008) 2283-2295.

34. F. Jiao, P.G. Bruce, *Adv. Mater.* 19 (2007) 657-660.

35. G. Girishkumar, B. McCloskey, A.C. Luntz, S. Swanson, W. Wilcke, *J. Phys. Chem. Lett.* 1 (2010) 2193-2203.

36. H. Li, H. Zhou, *Chem. Commun*. 48 (2012) 1201-1217.

37. R. Marom, S.F. Amalraj, N. Leifer, D. Jacob, D. Aurbach, *J. Mater. Chem.* 21 (2011) 9938-9954.

38. O. Haik, S. Ganin, G. Gershinsky, E. Zinigrad, B. Markovsky, D. Aurbach, I. Halalay, *J. Electrochem. Soc*. 158 (2011) A913-A923.

39. H. Wang, M. Yoshio, T. Abe, Z. Ogumi, *J. Electrochem. Soc.* 149 (2002) A499-A503.

40. H. Fujimoto, K. Tokumitsu, A. Mabuchi, N. Chinnasamy, T. Kasuh, *J. Power Sources* 195 (2010) 7452-7456.

41. J. Yang, X.-y. Zhou, J. Li, Y.-l. Zou, J.-j. Tang, *Mater. Chem. Phys.* 135 (2012) 445-450.

42. C.A. Bridges, X.-G. Sun, J. Zhao, M.P. Paranthaman, S. Dai, *J. Phys. Chem.* C 116 (2012) 7701-7711.

43. J. Ni, Y. Huang, L. Gao, *J. Power Sources* 223 (2013) 306-311.

44. V. Meunier, J. Kephart, C. Roland, J. Bernholc, *Phys. Rev. Lett.* 88 (2002) 075506.

45. C.M. Schauerman, M.J. Ganter, G. Gaustad, C.W. Babbitt, R.P. Raffaelle, B.J. Landi, *J. Mater. Chem.* 22 (2012) 12008-12015.

46. R.A. DiLeo, A. Castiglia, M.J. Ganter, R.E. Rogers, C.D. Cress, R.P. Raffaelle, B.J. Landi, *ACS Nano* 4 (2010) 6121-6131.

47. H.J. Hwang, J. Koo, M. Park, N. Park, Y. Kwon, H. Lee, *J. Phys. Chem. C* 117 (2013) 6919-6923.

48. D. Pan, S. Wang, B. Zhao, M. Wu, H. Zhang, Y. Wang, Z. Jiao, *Chem. Mater.* 21 (2009) 3136-3142.

49. B.P. Vinayan, S. Ramaprabhu, *J. Mater. Chem. A* 1 (2013) 3865e3871.

50. Y. Liu, Y. Qiao, W.-X. Zhang, Z. Li, X.-L. Hu, L.-X. Yuan, Y.-H.Huang, *J. Mater. Chem.* 22 (2012) 24026-24033.

51. L. Fei, Q. Lin, B. Yuan, G. Chen, P. Xie, Y. Li, Y. Xu, S.Deng, S. Smirnov, H. Luo, *ACS Appl. Mater. Interfaces* 5 (2013)5330-5335.

52. S.Y. Huang, X.Y. Liu, Q.Y. Li, J. Chen, *J. Alloys Compd.* 472 (2009) L9-L12.

53. S. Ding, D. Zhang, J.S. Chen, X.W. Lou, *Nanoscale* 4 (2012)95-98.

54. X. Wang, Z. Zhang, Y. Chen, Y. Qu, Y. Lai, J. Li, *J. AlloysCompd.* 600 (2014) 84-90.

55. Kobayashi. K, Yamauchi. J, *Physical Review B.* 51 (23) (1995), 17085-17095.

56. J. Li, Y. Hou, X. Gao, D. Guan, Y. Xie, J. Chen, C. Yuan, *Nano Energy* 16 (2015) 10-18.

57. J. Deng, H. Li, J. Xiao, Y. Tu, D. Deng, H. Yang, H. Tian, J. Li, P. Ren, X. Bao, ***Energy Environ. Sci.* 8 (2015)** 1594-1601 .

58. Zabinski, J. S., Donley, M. S., Walck, S. D., Schneider, T. R.,McDevitt, N. T. *Tribology Transactions* 38 (1995) 894–904.

59. H. M. Jeong, J. W. Lee, W. H. Shin, Y. J. Choi, H. J. Shin, J. K. Kang, J. W. Choi*, Nano letters* 11 (6) (2011) 2472-2477.

60. H. Wang, T. Maiyalagan, X. Wang, *Acs Catalysis* 2 (5) (2012) 781-794

61. P. Chen, J. J. Yang, S. S. Li, Z. Wang, T. Y. Xiao, Y. H. Qian, S. H. Yu, *Nano Energy* 2 (2) (2013) 249-256.

62. A. Huczko, *Appl. Phys. A* 70 (4) (2000) 365.

63. M. Arturo, L. Quintela, *Curr. Opin. Colloid Interface Sci.* 8 (**2003)** 137.

64. Kulkarni S., *Nanotechnology: Principles and Practices*, Third Edition, Springer, 2015.

65. J. Xu, H. Yang, W. Fu, K. Du, Y. Sui, J. Chen, Y. Zeng, M. Li, G. Zou, *J. Magn. Magn. Mater* 309 (2007) 307.

66. R. Chaudhuri, S. Paria, *Chem. Rev.* 112 (2012) 2373.

67. S. Verma, R. Gokhale, D. J. Burgess. *Int. J. Pharm*. 380 (2009) 216.

68. C. Hawker, T. Russell, *MRS Bulletin* 30 (2005) 952.

69. https://en.wikipedia.org/wiki/Sol%E2%80%93gel_process

70. https://en.wikipedia.org/wiki/Hydrothermal_synthesis

71. H. Chiu, C. Yeh. *J. Phys. Chem. C* 20 (2007) 111.

72. http://www.farnell.com/datasheets/1496885.pdf